Quaternary Science Reviews 257 (2021) 106771

Contents lists available at ScienceDirect

Quaternary Science Reviews

journal homepage: www.elsevier.com/locate/quascirev

The Zealandia Switch: Ice age climate shifts viewed from Southern Hemisphere moraines

George H. Denton [a], Aaron E. Putnam [a, *], Joellen L. Russell [b], David J.A. Barrell [c], Joerg M. Schaefer [d, e], Michael R. Kaplan [d], Peter D. Strand [a]

[a] School of Earth and Climate Science and Climate Change Institute, University of Maine, Orono, ME 04469, USA
[b] Department of Geosciences, University of Arizona, Tucson, AZ, USA
[c] GNS Science, Dunedin, New Zealand
[d] Lamont-Doherty Earth Observatory of Columbia University, 61 Rt 9W, Palisades, NY 10964, USA
[e] Department of Earth and Environmental Sciences, Columbia University, New York, NY 10027, USA

ARTICLE INFO

Article history:
Received 12 June 2020
Received in revised form
3 December 2020
Accepted 14 December 2020

Keywords:
Quaternary
Glaciation
Climate dynamics
Climate modeling
Paleoclimatology
Southern Ocean
South Pacific Ocean
Cosmogenic isotopes
Geomorphology
Glacial
Southern Hemisphere westerlies

ABSTRACT

Two fundamental questions about the ice-age climate system await satisfactory resolution. First, if summer solar radiation intensity truly controls the orbital signature of the last glacial cycle, then why were major climatic shifts, including the last termination, globally synchronous? Second, what caused the millennial-scale climate oscillations superimposed on this cycle? We address these questions from a Southern Hemisphere perspective focused on mid-latitude mountain ice fields. We put particular emphasis on the last glacial termination, which involved both orbital-scale and millennial-scale climate elements and has generally well-resolved chronological control.

Sustained retreat of mountain glaciers, documented by detailed mapping and chronology of glacial landforms in the Southern Alps and southern Andes, marked the termination of the last ice age, beginning ~18 kyrs ago and involved a change from glacial to near-interglacial atmospheric temperature within a millennium or two. A rapid poleward shift of the Subtropical Front, delineating the northern margin of the Southern Ocean, ~18 kyrs ago implies a concurrent poleward shift of the austral westerlies and leads us to hypothesize a southern origin for the dominant phase of the last glacial termination. Together with interhemispheric paleoclimate records and with results of coupled ocean-atmosphere climate modeling, these findings suggest a big, fast, and global end to the last ice age in which a southern-sourced warming episode linked the hemispheres. We posit that a shift in the Southern Ocean circulation and austral westerly wind system, tied to southern orbital forcing, caused this global warming episode by affecting the tropical heat engine and hence global climate.

Central to this hypothesis, dubbed the 'Zealandia Switch', is the location of the Australia and Zealandia continents relative to Southern Hemisphere oceanic and atmospheric circulation. Coupled ocean-atmosphere climate modeling shows that the locus of the austral westerlies, whether in a more equatorward position representing a glacial-mode climate or in a poleward-shifted position marking interglacial-mode climate, has profound effects on oceanic and associated atmospheric linkages between the tropical Pacific and the Southern Ocean. Shifts in the austral westerlies have global climatic consequences, especially through resulting changes in the greenhouse gas content of the atmosphere and altered heat flux from the tropical Pacific into the Northern and Southern Hemispheres. We suggest that the last glacial termination was a global warming episode that led to extreme seasonality in northern latitudes by stimulating a flush of meltwater and icebergs into the North Atlantic from adjoining ice sheets. This fresh-water influx resulted in widespread North Atlantic sea ice that caused very cold boreal winters, thus amplifying the annual southward shift of the Intertropical Convergence Zone and the monsoonal rain belts. We further suggest that muted manifestations of the Zealandia Switch mechanism were responsible for smaller, recurring millennial-scale climate oscillations within the last glacial cycle.

© 2020 Elsevier Ltd. All rights reserved.

* Corresponding author.
E-mail address: aaron.putnam@maine.edu (A.E. Putnam).

https://doi.org/10.1016/j.quascirev.2020.106771
0277-3791/© 2020 Elsevier Ltd. All rights reserved.

1. Ice age puzzles

Glacier moraines afford physical evidence of past climate variations. Over the last 25 years, our research team has mapped and established chronologies for moraines deposited by mountain glaciers during the last ice age and its termination in New Zealand's Southern Alps and in the southern Andes of South America. Here we use the results of those investigations to address long-standing puzzles that so far have hindered adequate understanding of climate behavior during and following the Last Glaciation.

One puzzle relates to a prominent theory of ice ages proposed by Murphy (1869) and developed by Milankovitch (1941) which attributes the formation and fluctuations of Pleistocene ice masses to changes in summer insolation intensity over the high-latitude northern continents resulting from variations in Earth's orbit. **A second puzzle** concerns the origin of prominent millennial-scale climate oscillations that occurred during the Last Glaciation, and were expressed, for example, as Heinrich stadials (HS) and Antarctic Isotope Maxima events (Rasmussen et al., 2014; Brook and Buizert, 2018).

As background, the Last Glaciation refers globally to the period approximately spanning Marine Isotope Stages (MIS) 4–2. The early cold episode of MIS 4 was followed by a climatic recovery at the start of MIS 3, then increasing growth of continental ice sheets through to MIS 2. A generally accepted definition of the Last Glacial Maximum (LGM) is "the time of the most recent maximum in globally integrated ice volume", coinciding with the maximal depression of eustatic sea level (Mix et al., 2001). This sea-level low stand was linked mainly to Northern Hemisphere ice sheets because Antarctic ice underwent relatively minor glacial/interglacial volume change (Denton and Hughes, 2002). Southern Hemisphere mountain ice fields also achieved maximal extents at about the same time (Mercer, 1984). From chronological data compiled from terrestrial and sea-level records, Clark et al. (2009) concluded that the Northern Hemisphere ice sheets achieved maximum extents between 26.5 and 19 kyrs ago. That time interval aligns with Antarctic temperatures inferred from ice cores that place the coldest Antarctic conditions of the Last Glaciation between 26 and 19 kyrs ago (Kawamura et al., 2007; Buizert et al., 2015; Cuffey et al., 2016). We consider the initiation of the last glacial termination as the onset of rapid environmental change, seen globally in many proxies, directly following the LGM ~18 kyrs ago.

With regard to the first puzzle, Hays et al. (1976) made a convincing case that orbital variation is the principal influence on climate shifts but did not take a position on its specific linkage to the global ice-age climate system. With regard to such linkage, explanations for glacial cycles and their terminations have commonly focused on an orbitally-induced 'northern' driver for glacial climate, underpinned by the Murphy (1869) and Milankovitch (1941) summer insolation concept. However, a difficulty with this linkage emerged when the dating of glacial deposits showed a global symmetry of episodes of glacier expansion/retreat (e.g., Mercer, 1976), rather than hemispheric asymmetry that would be expected if summer solar radiation intensity truly controlled glaciation (Huybers, 2009). Chronological results for glaciation in the Chilean Lake District of the Andes led Mercer (1976, 1984) to conclude that glacier expansion to a maximum during the last ice age, and demise at its end, occurred approximately in unison between mid-latitudes of the Southern and Northern Hemispheres, despite summer insolation intensity being anti-phased between the hemispheres. Mercer (1984) concluded that such simultaneous climatic change at the orbital timescale in both hemispheres "defies satisfactory explanation". Broecker (1978) described this conundrum as "a fly in the insolation ointment", which we refer to here as Mercer's Paradox.

Further complications have arisen from increasingly detailed chronologies of former glacier extents in Southern Hemisphere middle latitudes in South America and New Zealand (this paper; Denton et al., 1999; Schaefer et al., 2006, 2015; Doughty et al., 2015; Kelley et al., 2014; Strand et al., 2019). These moraine chronologies indicate that Southern Hemisphere glaciers had recurring maxima of similar extent not only during the global LGM in MIS 2, but also in the MIS 3 and MIS 4 intervals. In several cases, the greatest ice extents were attained prior to the global LGM. The chronological results emphasize that middle-latitude mountain glaciers in the Southern Hemisphere during the course of the last ice age and its demise did not fluctuate in concert with orbitally-induced local summer insolation variations. Thus the summer-orbital mechanism applied by Murphy (1869) and Milankovitch (1941) to Northern Hemisphere ice sheets seems not to have worked for mid-latitude Southern Hemisphere mountain glaciation. Further, the episodes of southern mid-latitude glacier fluctuations also bear upon the second puzzle that relates to the origin of millennial-scale climate variability. The emerging pattern of southern glacier fluctuations mimics, in an anti-phased way, the occurrence of northern Heinrich stadial episodes (Strand et al., 2019).

The orbital- and millennial-scale ice-age puzzles are illustrated collectively by events early in the last glacial termination, dubbed the Mystery Interval by Denton et al. (2006). Beginning shortly after 18 kyrs ago, mountain glaciers in both the Southern Alps and the southern Andes underwent sustained recession. At the same time in the Northern Hemisphere, an intense millennial-scale Heinrich Stadial climatic episode (HS1) was manifested in different ways across a range of climatic proxies (Barker et al., 2009; Hodell et al., 2017). HS1 was associated with discharge of icebergs from both sides of the North Atlantic, referred to as Heinrich Event 1 (Bond et al., 1992; Broecker et al., 1992; Bond and Lotti, 1995; Grousset et al., 2001). HS1 was characterized by exceptionally cold northern winters (Denton et al., 2005; Buizert et al., 2014) and was accompanied by widespread North Atlantic sea ice (Isarin et al., 1998), and minimal sea-surface temperatures in some sectors of the North Atlantic (Bard et al., 2000; Rasmussen et al., 2016). HS1 was also marked by distinctive isotopic signatures and enhanced aeolian dust deposition in Greenland ice (Mayewski et al., 1997; Stuiver and Grootes, 2000), and reduced intensity of the Asian monsoon (Wang et al., 2001). It is noteworthy that Heinrich events in the North Atlantic, including that during HS1, were coeval with warm and wet climate episodes in Florida (Grimm et al., 2006). HS1 recession of northern ice sheets resulted in sea-level rise of ~20 m (Stanford et al., 2011) while Antarctic ice was maintaining its LGM position (Hall et al., 2015). A particularly puzzling feature of HS1 is that mountain glaciers in the European Alps underwent rapid and substantial recession early in HS1 (e.g., Wirsig et al., 2016a) despite the occurrence of a regional cold stadial.

In seeking to account for Mercer's Paradox, Denton et al. (2010) hypothesized that the termination of the last glacial cycle was initiated through a widely-suggested northern orbital driver, whereby glacial-maximum full-bodied Northern Hemisphere ice sheets were destabilized by increasing summer insolation intensity. Warming-induced collapse of ice-sheet margins produced meltwater that fueled a strong northern stadial (Denton et al., 2005). That in turn induced a southward shift of atmospheric circulation zones, notably the austral westerlies, which invigorated Southern Ocean circulation producing southern warming and the release there of deep-sea CO_2. Rising atmospheric CO_2 afforded a global warming feedback that helped to lock in a climate shift to global interglacial conditions.

A difficulty with the Denton et al. (2010) mechanism is the notable lack of correlation between orbitally-induced local summer intensity and advance/recession of middle-latitude Southern

Hemisphere ice fields during MIS 4, 3, and 2. Such a striking discrepancy raises the question of whether summer insolation intensity is as important a control on ice-body behavior as has been thought, in either hemisphere. This invites consideration of whether other expressions of orbital variation, such as the duration of seasons in the Southern Hemisphere (Huybers and Denton 2008), could have driven interhemispheric climatic effects. This issue was foreshadowed by Putnam et al. (2013b) who proposed that the influence of orbitally-controlled seasonal duration on Southern Ocean stratification may have been a fundamental modulator of Southern Hemisphere mid-latitude glaciation, although they still suggested a northern driver for the last glacial termination.

Here, we take a new look at Mercer's Paradox, by drawing upon ever-improving chronologies of mid-latitude Southern Hemisphere mountain-glacier moraines as physical evidence and sensitive recorders of climatic variation. We examine the southern glacial landform chronologies in the context of Antarctic climatic signatures and of physical evidence of glacier extent based on moraines in the mid-latitude Northern Hemisphere. Noting that the southern mid-latitude icefields lie adjacent to the northern sector of the Southern Ocean, we combine our interpretation of moraine chronologies with modeling that simulates the effects of shifting the latitude and strength of the austral westerlies over the Southern Ocean. We use these lines of evidence to assess whether oceanic and atmospheric factors in the Southern Hemisphere ('southern' driver) had important roles in global ice-age climate shifts.

2. Southern mid-latitude moraine chronologies

There is a considerable body of chronological data pertaining to past glacier extent in the Southern Hemisphere mid-latitudes, for example as summarized for southern South America by Davies et al. (2020) and Palacios et al. (2020) and outlined for New Zealand by Barrell (2011), Barrell et al. (2013), Shulmeister et al. (2019), and Eaves and Brook (2021). In Australia, Quaternary glaciation was confined to localized parts of Tasmania and the Snowy Mountains in the far southeast of the continent (e.g., Colhoun and Barrows, 2011). Glaciers there existed under glacial climate but none survived the most recent transition to interglacial climate (Colhoun and Barrows, 2011), unlike New Zealand and South America where glaciers locally persist to the present day.

Here we summarize moraine chronologies obtained by our research group in the mid-latitude sector of the South American Andes and in New Zealand's Southern Alps (Fig. 1), the two main locales of Southern Hemisphere mid-latitude mountain glaciation. The focus on our research group's work arises from our detailed familiarity with the geomorphic setting and context of the dating targets, and because the surface-exposure dating used identical sampling, processing and analytical procedures, and the same accelerator mass spectrometer (Section 2.1).

For our research work, geomorphic maps of glacial landforms provided a foundation for the chronological investigations (Andersen et al., 1999; Denton et al., 1999a; Barrell et al., 2011), accompanied in the Chilean Lake District by study of stratigraphic sections of glacial deposits (Denton et al., 1999b). The chronological studies include ^{10}Be surface-exposure chronologies for moraine landform sequences in several valleys on the eastern side of the Southern Alps (Schaefer et al., 2009, 2015; Kaplan et al., 2010, 2013; Putnam et al., 2010a,b, 2012, 2013a,b; Kelley et al., 2014; Doughty et al., 2015; Strand et al., 2019) and a radiocarbon chronology of Last Glaciation moraine deposits in the Chilean Lake District on the western side of the Andes (Denton et al., 1999a, 1999b; Moreno et al., 2015).

2.1. Southern Alps moraine chronologies

We investigated moraine sequences in three major southeast-draining valley systems: Pukaki, Ohau, and Rakaia. The Pukaki valley has well-preserved glacial landforms (Figs. 2 and 3). Post-glacial Lake Pukaki lies in the trough of the ice-age Pukaki glacier (Barrell and Read, 2014) which, during ice-age maxima, flowed southward for ~75 km from the highest sector of the Southern Alps (Fig. 4). The glacier formed a complex of moraines adjacent to its lateral and terminal margins, with associated kame terraces and outwash plains. The Pukaki moraine-outwash complex is differentiated into several morphostratigraphic groups (Fig. 3) named, from oldest to youngest, Wolds, Balmoral, Mt. John, and Tekapo (Speight, 1963; Barrell, 2014; Barrell and Read, 2014). Birch Hill moraines, of late-glacial age, and Holocene moraines lie farther up the catchment (Schaefer et al., 2009; Putnam et al., 2010a; Barrell et al., 2011; Kaplan et al., 2013). The morphostratigraphic subdivision is based on differences in landform preservation, relative positions within the catchment and landform sequences, and cross-cutting geomorphic relationships. This same morphostratigraphic classification also applies to glacial landforms in the adjacent Lake Ohau catchment, whose geological and geomorphological setting is analogous to that of the Pukaki catchment (Kaplan et al., 2010; Putnam et al., 2013b). Different morphostratigraphic names are used in the Rakaia River catchment about 120 km northeast of Lake Pukaki (Putnam et al., 2012, 2013a). Longitudinal profiles of the former Rakaia, Pukaki and Ohau glacier valleys, together with dating results (Fig. 4), summarize the Last Glaciation and deglacial history of these catchments.

Quantitative dating investigations using in-situ-produced cosmogenic nuclides (surface exposure dating) targeted large erratic boulders of greywacke protruding from moraine surfaces (see Appendix 1). Samples were collected following the procedures outlined in Putnam et al. (2010b) and processed at the Lamont-Doherty Earth Observatory Cosmogenic Dating Laboratory for ^{10}Be analysis (see Schaefer et al., 2009). ^{10}Be/^{9}Be ratios were measured at Lawrence-Livermore National Laboratory, with corrections for background ^{10}Be measured in procedural blanks (typically <1%). A locally established production-rate calibration for ^{10}Be was used in the age calculations (Putnam et al., 2010b). All moraine ages discussed in this paper are expressed as arithmetic means of ^{10}Be age populations with 'external uncertainties'. External uncertainties were calculated for each age population by propagating the standard error of the mean with a systematic 2.1% production-rate uncertainty (see Appendix 1 for details). Sample details and ages for the Last Glaciation and late-glacial moraine belts of the Pukaki valley (excluding tributaries) are presented in Tables S1 and S2 (Supplementary data), with previously published ages updated to include external uncertainties. Probability distributions for individual ages and the mean age for each moraine belt are plotted in Fig. A1 in Appendix 1. Samples with ages that are inconsistent relative to their morphostratigraphic location, or relative to the majority of other ages from the same landform feature, are classified as outliers and excluded from moraine age calculations. All samples described by Schaefer et al. (2006) have been remeasured at Lawrence-Livermore National Laboratory and ages recalculated on the same basis as the other ^{10}Be ages presented here. ^{10}Be exposure ages are expressed as years before A.D. 1950, to enable direct comparison to radiocarbon ages. In the discussion of moraine ages below, 'n' denotes the number of ages excluding outliers. Landform ages and uncertainties are reported according to the conventions of Stuiver and Polach (1977), and presented in rounded form in Table S3 (Supplementary data).

In addition to previously published results (Schaefer et al., 2006, 2015; Putnam et al., 2010a, 2010b; Kelley et al., 2014; Doughty et al.,

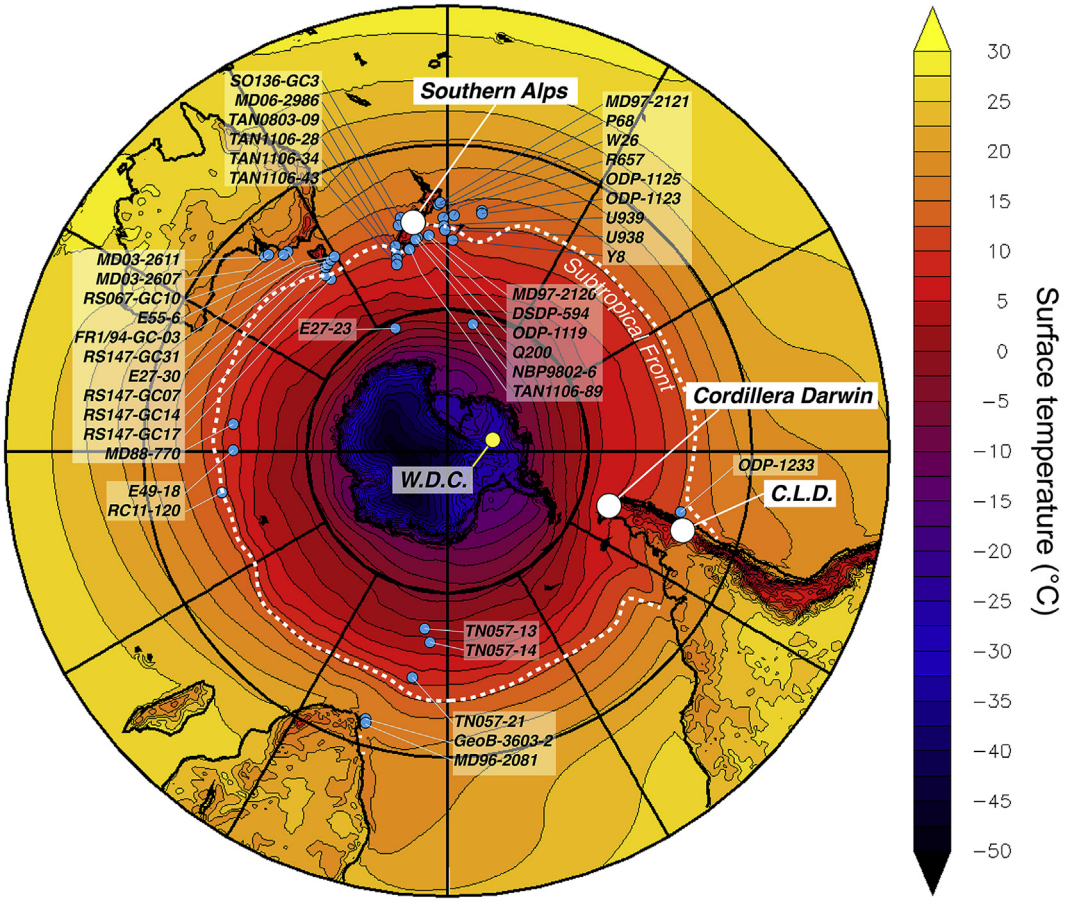

Fig. 1. Map of the southern sector of the Southern Hemisphere. Surface temperature isotherms are shown as 1 °C color bands, with the locations of marine cores (blue-filled circles), WAIS Divide ice core (W.D.C.; yellow-filled circle), and terrestrial glacial geologic field areas (white-filled circles) mentioned in the text (C.L.D. = Chilean Lake District). Over the Southern Ocean, the isotherms approximate sea surface temperatures. The white dotted line represents the approximate position of the Subtropical Front. (For interpretation of the references to color in this figure legend, the reader is referred to the Web version of this article.)

2015; Strand et al., 2019), the Pukaki valley moraine chronology presented here includes 53 new ages, comprising 16 from the inner Mt John moraines, 32 from the Tekapo moraines, and five from deglacial landforms. The exposure ages of the Pukaki moraine sequence (Fig. 3) are: Balmoral, 65,100 ± 1400 yrs, n = 45 (Schaefer et al., 2015); Mt. John, within which at least five different episodes of moraine formation are identified, from oldest to youngest, 44,000 ± 1100 yrs, n = 8 (Strand et al., 2019); 41,760 ± 940 yrs, n = 14 (Kelley et al., 2014; Strand et al., 2019); 36,640 ± 870 yrs, n = 12 (Kelley et al., 2014; Doughty et al., 2015; Strand et al., 2019); 27,000 ± 620 yrs, n = 16 (Kelley et al., 2014; Doughty et al., 2015; Strand et al., 2019); 20,310 ± 440 yrs, n = 54 (Kelley et al., 2014; Doughty et al., 2015; Schaefer et al., 2015; Strand et al., 2019); and Tekapo, 18,110 ± 380 yrs, n = 57 (Putnam et al., 2010b; Kelley et al., 2014; Doughty et al., 2015). The late-glacial Birch Hill moraines (Fig. 3) (Putnam et al., 2010a) comprise an outboard knob (14,140 ± 300 yrs, n = 2), and a prominent semi-continuous lateral ridge with a set of inboard discontinuous recessional ridges (Appendix 2). Samples from the lateral ridge and the recessional ridges gave ages that are all indistinguishable within error and yield a combined age of 13,010 ± 280 yrs, n = 21. In the Whale Stream tributary valley, a total of 10 samples from a large late-glacial moraine complex, located within 3 km of Late Holocene moraines, range in age from 15,400 ± 400 to 12,900 ± 500 yrs (Kaplan et al., 2013). We present five new dating results for erratic boulders on an ice-molded hill, just outboard of the Birch Hill moraine belt (Figs. 3 and 4), with a mean age of 17,480 ± 430 yrs, n = 5. The difference between the maximum age bound of the Birch Hill moraines (13,290 years) and the minimum age bound of the erratic boulders (17,050 years) implies that at least 3760 yrs elapsed between the hill's emergence from beneath the retreating Pukaki glacier and the ice resurgence that formed the Birch Hill moraines.

In the Ohau valley, the moraine sequence contains six landform sets with distinctive morphostratigaphic and chronological characteristics (Putnam et al., 2013b) (Figs. 3 and 4). The outer part of the Mt. John belt yielded an age of 32,520 ± 790 yrs, n = 6. Moraine remnants a little farther up the valley afforded individual ages of 28,300 ± 1200 and 26,400 ± 1000 yrs, n = 2. Slightly farther up the valley is a nearly continuous moraine belt that gave an age of 22,510 ± 6490 yrs, n = 24. Adjacent to the lake is the Tekapo moraine belt with its associated inset outwash plain (Fig. 3). The outer sector of this moraine belt returned an age of 18,220 ± 400 yrs, n = 18, whereas the inner sector yielded an age of 17,690 ± 400 yrs, n = 6. About 24 km up valley (north) of the inner Tekapo moraines, boulders dropped on an ice-molded hill by the receding Ohau glacier gave an age of 17,380 ± 400 yrs, n = 7. In the Irishman Stream tributary valley, prominent late-glacial moraines include an outer ridge dated to 13,000 ± 290 yrs ago, n = 9, and an innermost ridge formed 11,500 ± 300 yrs ago, n = 5 (Kaplan et al., 2010).

In the Rakaia valley, dating of moraines and ice-molded landforms (Putnam et al., 2013a) shows that the ice-age Rakaia glacier

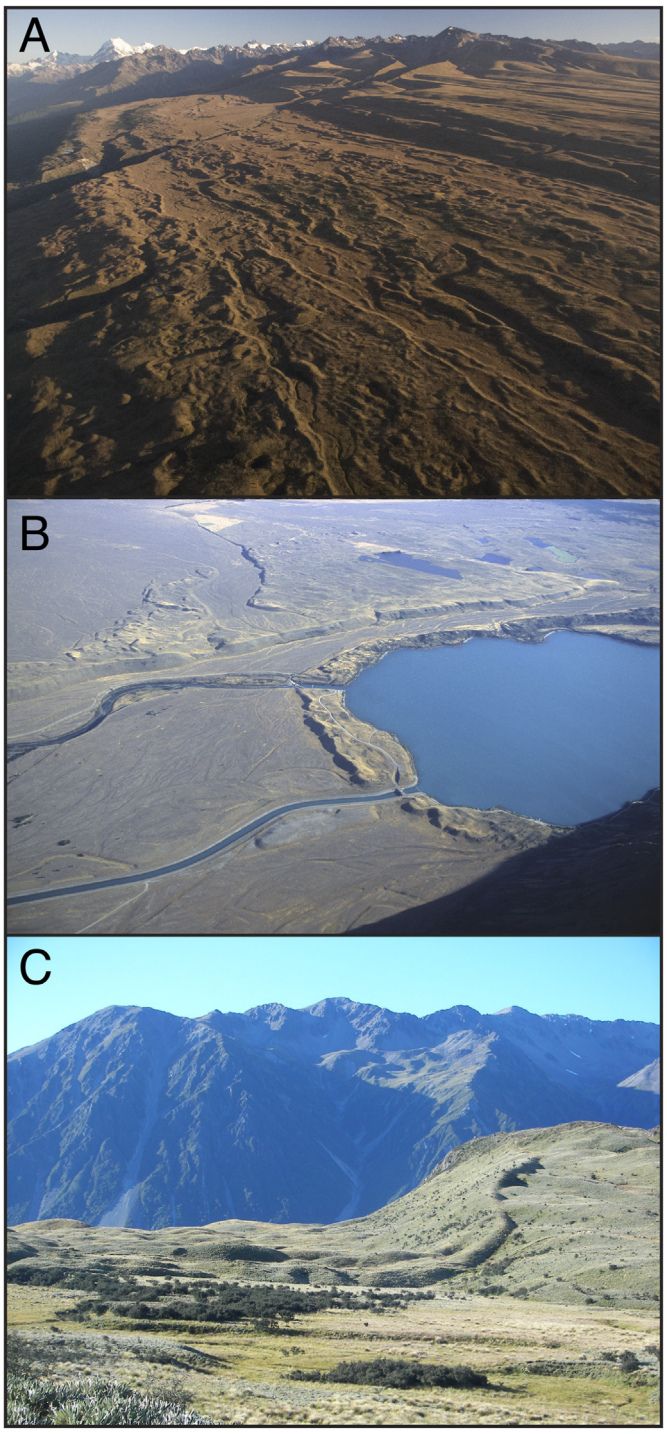

Fig. 2. Aerial views of examples of moraine belts formed by Southern Alps glaciers. A) Belts of left-lateral moraines deposited by the Pukaki glacier between ~65 kyrs and ~18 kyrs ago. Vantage is to the north (see Fig. 3). B) ~18-kyr lakeside moraine belt at Lake Ohau (from Putnam et al., 2013b). The construction of this belt culminated shortly before the onset of the termination. Vantage is to the south (see Fig. 3). C) ~16-kyr moraine at Prospect Hill in the upper Rakaia valley, deposited following extensive recession of the Rakaia glacier between 18 and 17 kyrs ago. Vantage is to the north.

began sustained retreat from a prominent moraine ridge at about 17,840 ± 390 yrs ago, n = 5), with erratic boulders immediately inboard of the ridge of similar age (17,960 ± 410, n = 3). At that time, the glacier terminus was at least 70 km down-valley of the Late Holocene terminal moraines in the headwaters (Fig. 4). The glacier had receded from Double Hill, within 42 km of the Late Holocene moraine position, by 16,960 ± 390 yrs ago, n = 5 and had withdrawn at least a further 12 km up-valley, prior to the construction of a moraine at Prospect Hill 16,250 ± 360 yrs ago, n = 8. By 15,660 ± 350 yrs ago, n = 2, glacier ice was at, or behind, the location of a complex of lateral moraines and meltwater channels that yielded ages of 14,850 ± 340 yrs, n = 3 (Putnam et al., 2013a), 13,900 ± 300 yrs, n = 4, and 13,140 ± 300 yrs, n = 5, (Koffman et al., 2017). About 2 km farther up-valley and at lower elevation are two closely-spaced moraine belts, the higher of which was formed at 12,140 ± 260 yrs ago, n = 8, and the lower formed 11,620 ± 250 yrs ago, n = 5 (Koffman et al., 2017).

Despite being in adjacent catchments, the Ohau and Pukaki sequences contain some full-glacial moraines of different ages. These differences most likely reflect random variations in moraine preservation due to erosion or overprinting issues, coupled with contrasts in the morphometry and altitudinal geometry in each catchment, its trunk valley and proximal foreland. We consider it appropriate to combine the moraine-forming episodes into a composite record, thus identifying central Southern Alps ice advance to full-glacial extent at ~44, ~42, ~37, ~33-32, ~27, ~23-22, ~20 and ~18 kyrs ago (Table S3, Supplementary data). Moraines formed ~18 kyrs ago are prominent in the Ohau, Pukaki, and Rakaia valleys, because those moraines represent the last advance prior to the termination and thus are widely preserved. Major and sustained ice recession, initiated shortly after ~18 kyrs ago, is registered in all three catchments. In the Rakaia valley and at Whale Stream, moraines were formed at about the late-glacial position as early as ~16 kyrs ago in the Rakaia valley, and at both locations between ~15 kyrs and ~13 kyrs ago. In the Pukaki valley, ~13 kyr old moraines appear to have almost entirely overprinted evidence of earlier late-glacial ice margins. Moraine records from the Ohau and Rakaia catchments document progressive ice recession between ~13 and ~11.5 kyrs ago, during HS0 (Younger Dryas) time (Kaplan et al., 2010; Koffman et al., 2017).

2.2. Southern South America moraine chronologies

The Last Glaciation Llanquihue moraine belt of the Chilean Lake District (Fig. 1) and of Isla Grande de Chiloe was formed by outlet lobes of the northern sector of an extensive Patagonian Ice Sheet. Organic sediments buried by or resting on glacial deposits have yielded a radiocarbon chronology of ice advances or retreats within the terminal moraine belts (Denton et al., 1999a, 1999b; Moreno et al., 2015) (see Fig. 7). All previously published radiocarbon ages referred to in this paper are stated in calendar years B.P. according to IntCal13 (Reimer et al., 2013; Moreno et al., 2015). Major advances of the Lago Llanquihue lobe occurred at 33.6 ± 0.2 kyrs ago, n = 5, and 30.8 ± 0.1 kyrs ago, n = 9. The Seno Reloncavi lobe registered a major advance at 26.9 ± 0.2 kyrs ago, n = 4, coeval with an advance of the Corcovado lobe at 26.8 ± 0.2 kyrs ago, n = 9. Radiocarbon dates of organic matter from the base of several mires show ice evacuation of the Llanquihue moraine belt outboard of Lago Llanquihue at ~25 kyrs ago. The youngest advance into the Llanquihue moraine belt culminated at 18,100–17,890 yrs ago. A warmer episode, known as the Varas Interstade (Mercer, 1984; Denton et al., 1999a, 1999b), recorded in till stratigraphy and also in palynological records, immediately preceded the last advance into the Llanquihue moraine belt (Moreno et al., 2015). We do not regard the Varas episode as marking the termination because the vegetation and glaciers had returned to full-glacial configurations by ~18 kyrs ago (Denton et al., 1999b; Moreno et al., 2015).

Extensive deglacial recession from the Llanquihue moraine belts commenced shortly after ~18 kyrs ago. In the northern sector of the Chilean Lake District, the areal distribution of a widespread

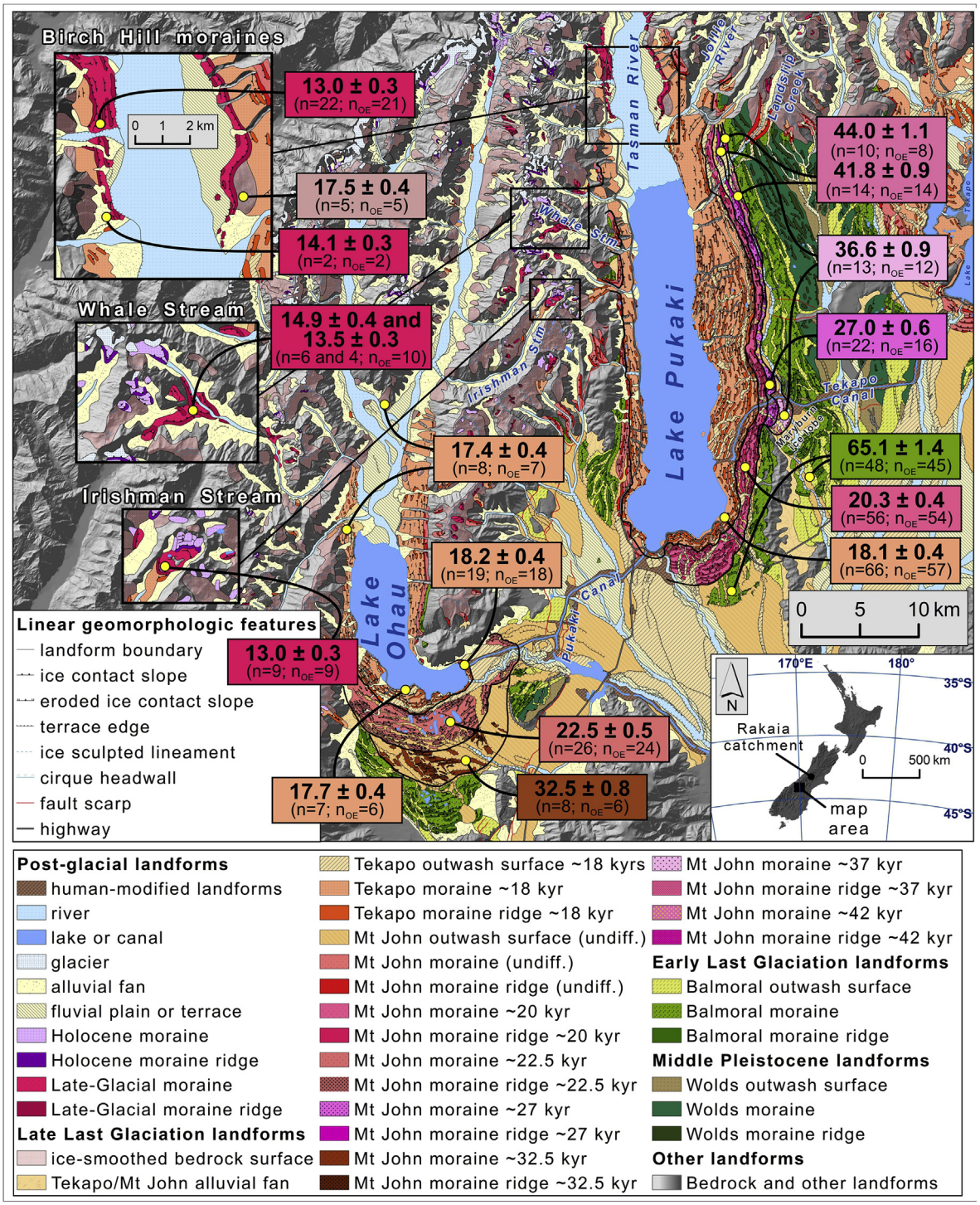

Fig. 3. Glacial geomorphic map of the Pukaki and Ohau moraine systems. Colored units correspond to different episodes of moraine formation, each of which has been dated using ^{10}Be. Moraine belt ages (in kyrs) are described in legend and given in colored boxes. Colored boxes present arithmetic mean ages with 'external' uncertainties (standard error of the mean propagated with a production-rate uncertainty of 2.1%) for each moraine belt, with n = the total number of samples dated, excluding replicates, and n_{OE} = the number of samples, excluding outliers and replicates, from which the mean was calculated (see Table S3). Yellow dots denote a representative location for each dated moraine belt. The Mount John ~42 kyr moraine unit includes the ~44-kyr moraines (Strand et al., 2019). The inset maps are at a common scale (refer to Birch Hill inset for scale bar). A high-resolution version of this figure is available in the Supplementary data. (For interpretation of the references to color in this figure, the reader is referred to the Web version of this article.)

ignimbrite deposit demonstrates that ice there had retreated far into the mountain valleys by 16,761 ± 109 yrs ago (Moreno et al., 2015). Farther south, on the eastern side of the Andes, radiocarbon dates of a detrital peat clast in till indicate that the Lago Argentino lobe of the Patagonian Ice Sheet had receded inboard of its Puerto Bandera late-glacial moraine by ~16 kyrs ago, prior to expansion to its maximum late-glacial position at ~13 kyrs ago and subsequent oscillating retreat (Strelin et al., 2011). In southernmost South America, extensive recession of the Patagonian Ice Sheet had occurred by 16,840 ± 350 yrs ago and by ~17,000 yrs ago

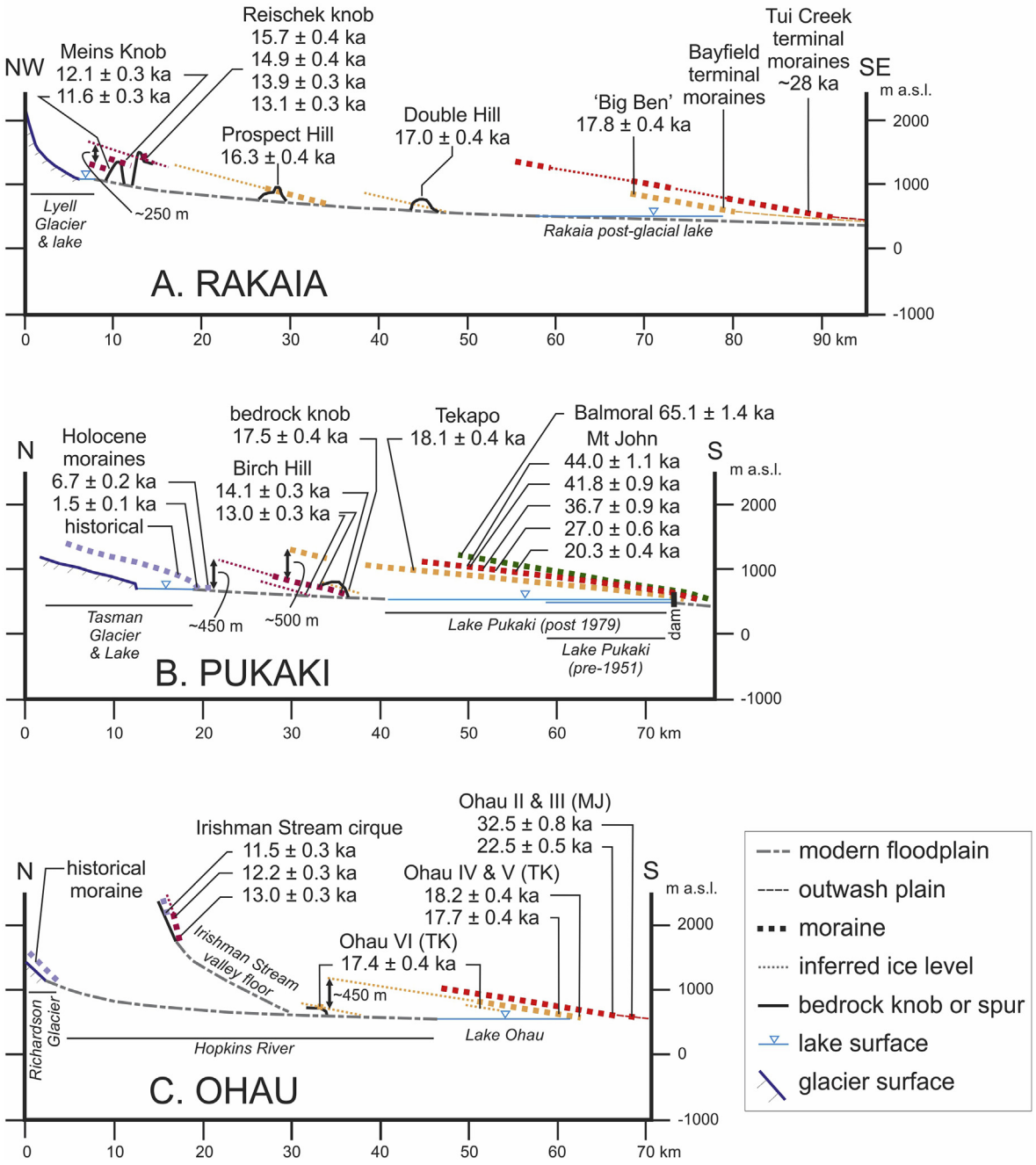

Fig. 4. Geomorphic profiles of the Rakaia (A), Pukaki (B) and Ohau (C) valleys, with valley axis distances in kilometers and elevations above sea level in meters. Mean landform ages are discussed in the text. Elevation changes of Lake Pukaki are described by Barrell and Read (2014), and construction of the Pukaki valley profile is discussed in Appendix 2. In C, the numbered Ohau moraine belts are from Putnam et al. (2013b), while the MJ and TK labels provide linkage to the Mt John and Tekapo moraine nomenclature.

respectively in the southern and northern parts of the Cordillera Darwin (Hall et al., 2013, 2019).

There is an extensive body of chronological data, especially surface exposure ages, pertaining to past extents, deglacial recession, and late-glacial advances of the Patagonian Ice Sheet and independent mountain glaciers (e.g., Davies et al., 2020 and references therein). Rapid recession of ice after ~18 kyrs ago is prominently illustrated in the datasets. In one example from the eastern margin of the North Patagonian Ice Field, Boex et al. (2013) document notable ice thinning and recession between ~ 18.1 and ~15.5 kyrs ago from near the maximum Last Glaciation extent to near the present-day position.

2.3. Climatic interpretation of Southern Hemisphere moraine sequences

The moraine records of the Southern Alps and western mid-latitude sector of the Andes are interpreted as physical evidence for atmospheric temperature prevailing at the time of moraine formation, particularly during the summer ablation season. This interpretation is commensurate with the temperate maritime setting of these regions and equates with the dominant control that temperature provides for present-day glaciers in the Southern Alps, for example (Anderson, 2005; Anderson et al., 2006; Anderson and Mackintosh, 2006; Anderson et al., 2010; Anderson and

Mackintosh, 2012; Lorrey et al., 2014; Purdie et al., 2014; Koffman et al., 2017) (see Appendix 2). Indeed, Mackintosh et al. (2017) concluded that the world's most temperature-sensitive modern mountain glaciers are located in the Southern Alps and in Patagonia. Morphostratigraphic breaks between Last Glaciation moraine belts, as expressed in the Pukaki, Ohau, and Rakaia landform sequences, imply that the glaciers pulled back from their lateral and terminal moraine margins between episodes of moraine formation. This suggests that there were variations in net atmospheric temperatures during the Last Glaciation. Glaciological modeling that applied precipitation values ranging from 0% to 30% less than present suggests that mean annual temperatures between ~6° and ~7 °C cooler than present were necessary for the Pukaki, Ohau and Rakaia glaciers to equilibrate at fully extended positions in their Last Glaciation moraine belts (Golledge et al., 2012; Putnam et al., 2013a, 2013b).

A prominent feature of the Southern Alps glacier record is the extensive ice recession that began ~17.8 kyrs ago and marked the local termination of the Last Glaciation. The three Southern Alps glacier systems discussed here had reduced at least 40% in length by ~17 kyrs ago. It has been hypothesized that proglacial lakes initiated at the last glacial termination in the main glacier valleys in the Southern Alps influenced glacier behavior through calving-induced rapid recession that decoupled the glacier trunks from climate-determined mass balance controls (e.g., Sutherland et al., 2019a, 2020). Similar interpretations have been made in relation to some southern South American glacial valleys (e.g., Bendle et al., 2019). In relation to the Southern Alps, the hypothesis appears to be largely predicated on the observation of rapid recession of relatively small contemporary valley glaciers since the mid-20th century. In the Rakaia valley, Shulmeister et al. (2010) pointed to an abundance of lateral ice-marginal landform features, in conjunction with surface exposure dating, to argue for progressive gradual ice recession following the last glacial termination. In contrast, surface exposure dating by Putnam et al. (2013a) showed the ice recession was rapid but nevertheless an array of ice-marginal landforms was constructed during recession. That recessional landform signature is characteristic of the margins of many of the main valley glacier troughs east of the central Southern Alps (Barrell et al., 2011). Surface-exposure dating shows the characteristic landform signature was formed during rapid ice recession in the Rangitata valley (Barrell et al., 2019a,b; Shulmeister et al., 2019b), Pukaki valley (this paper) and the Ohau valley (Putnam et al., 2013b). We consider that the signature of flights of lateral ice marginal features, typically dominated by kame terraces and lateral moraine ridges, descending gently to merge into the glacier trough, indicates formation alongside an active glacier margin undergoing an orderly progressive retreat, rather than catastrophic calving collapse associated with a floating glacier trunk, as envisioned by the ice-calving retreat hypothesis. Calving and iceberg production was very likely a feature of lake-terminating glacier termini during the last termination, for example shown by the stratigraphic evidence for ice-rafted debris documented for Lake Pukaki by Barrell and Read (2014). However, iceberg production could have occurred by processes such as thermal notch development as described at contemporary Lake Tasman by Röhl (2006), rather than necessarily requiring a floating glacier trunk. While calving processes could have hastened the recession of a glacier tongue terminating in a deep proglacial lake, evidence from Southern Alps glaciers that were not lake-terminating shows that any such effects were minor. The Mackenzie valley of the Ben Ohau Range, ~10 km west of Lake Pukaki, was occupied by a LGM glacier ~9 km long, with an average valley axis gradient of ~125 m fall per kilometer. Surface exposure dating by Dowey (2015) showed that during the last glacial termination, the glacier trunk had receded in length at least 75% by ~16.7 kyrs ago. The ~16.7-kyr ice-molded bedrock surface is onlapped by a ~14.1-kyr late-glacial terminal moraine. The chronological record from Mackenzie valley, which is too steep to have contained a proglacial lake, reinforces the view that the chronological record of recession from the major glacier valleys east of the central Southern Alps is predominantly an atmospheric climatic signature. On that basis, we consider that the chronology of moraines in the Ohau, Pukaki, Rakaia, and other similar valleys, can be interpreted as a primary climatic record, and infer that the same view generally applies elsewhere to major LGM mountain valley glaciers discussed in this paper.

On the assumption that the moraine chronological record is primarily a reflection of atmospheric temperature, Fig. 5 illustrates the changes in temperature during the termination, derived from glacier modeling based on the glacial-geological mapping and exposure dating (see Appendix). Modeling of the mapped and dated constraints on ice limits indicates atmospheric warming of at least 3.75 °C between ~17.8 and ~16.5 kyrs ago, representing at least 75% of the total Last Glaciation to Early Holocene temperature change. In a similar vein, Eaves et al. (2017) documented that ice in the Otira/Taramakau River catchment, located in the Southern Alps ~50 km north of the Rakaia valley, underwent massive recession in the interval between 17 and 15 kyrs ago during HS1, implying a rise in atmospheric temperature of at least 3 °C. In the upper Ohau, Rakaia and Pukaki catchments, late-glacial moraines formed during the interval between ~15.5 and ~13 kyrs ago, and represent stabilizations, or resurgences, of cirque and valley glaciers. Modeling indicates that those ice positions equate to mean annual temperature between ~2° and ~3 °C cooler than present (Kaplan et al., 2010, 2013; Putnam et al., 2010a; Doughty et al., 2013).

The Southern Alps moraine record is compatible with other paleoclimate proxies from the New Zealand region. Episodes of moraine formation correlate with intervals of cooler sea surface temperatures (SSTs) identified in marine core MD97-2120 (Pahnke et al., 2003; Doughty et al., 2015). Since 30 kyrs ago, moraine formation occurred during stadials defined from other proxies, notably pollen (Barrell et al., 2013; Lorrey and Bostock, 2017). Rapid ice recession beginning ~17.8 kyrs ago matches tightly with a

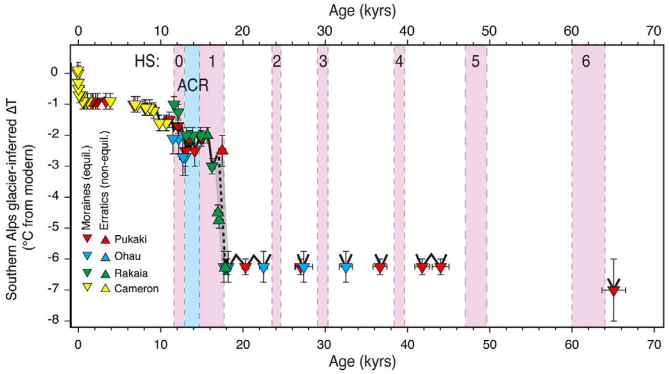

Fig. 5. Glacier-derived temperature reconstruction for the past ~70 kyrs. Chronology is based on surface-exposure dating of Southern Alps glacial landforms (Supplementary data; Tables S2 and S3). Temperature deviations (expressed as °C below modern) are derived using a combination of glaciological modeling and snowline-reconstruction techniques (Appendix 2). Upward-pointing arrows represent ages of landforms/boulders that were deposited during periods of glacier recession, and downward-pointing arrows represent ages of 'constructional' landforms that were deposited at the culminations of glacier advances. Triangle colors correspond to field area, given in legend. Grey envelope indicates the range of possible deglacial warming rates inferred from Pukaki and Rakaia landform chronologies. Pink vertical bands correspond to Heinrich Stadials in the North Atlantic. Blue vertical band corresponds to the Antarctic Cold Reversal/Bølling-Allerød interval. (For interpretation of the references to color in this figure, the reader is referred to the Web version of this article.)

recovery from grass-rich pollen spectra to near-interglacial woody vegetation at lowland sites on the western side of the Southern Alps (Vandergoes et al., 2013), and rapid warming of SSTs south of New Zealand, interpreted as a southward shift of the southern margin of the Subtropical Front (STF) (Bostock et al., 2015) (Fig. 6).

Advance of Chilean glacier lobes into the Last Glaciation moraine belts was associated with mean annual temperatures about 6 °C cooler than present (Denton et al., 1999a, 1999b). Ice recession after ~18 kyrs ago in southern South America was similar in scale and timing to that in the Southern Alps (Moreno et al., 2015). Furthermore, both the SST and the oxygen-isotope values from core ODP 1233, located just offshore of the Chilean Lake District (Fig. 1), show a major shift toward interglacial values concurrent with glacial recession onshore (Fig. 7). Supporting palynological evidence indicates that the tree line in the mid-latitude Chilean Lake District rose by 750 m (80% of the total glacial/interglacial rise) between ~17,800 and ~16,800 yrs ago (Moreno et al., 2015).

There has been much discussion of the role of the austral westerlies on Southern Hemisphere climate, and in particular the question of coupling between the position and strength of the westerlies and ocean temperatures and dynamics (e.g., Heusser, 1989; Lamy et al., 1998; Moreno et al., 1999; Lamy et al., 2004; Mohtadi and Hebbeln, 2004; Shulmeister et al., 2004; Kaiser et al., 2005; Kaplan et al., 2004; Mayewski et al., 2005; Toggweiler et al., 2006; Barrows et al., 2007; Lamy et al., 2007; Kaplan et al., 2008a,b; Toggweiler and Russell, 2008; Anderson et al., 2009; Toggweiler, 2009; Denton et al., 2010; Kaplan et al., 2010; McGlone et al., 2010; Putnam et al., 2010a; Burke and Robinson, 2012; McKay et al., 2012; Putnam et al., 2012; Boex et al., 2013; Kohfeld et al., 2013; Putnam et al., 2013a,b; ; Allen et al., 2015; Fogwill et al., 2015; Darvill et al., 2016; Markle et al., 2017; Mayewski et al., 2017; Garcia et al., 2018; Shulmeister et al., 2018; Bendle et al., 2019; Shulmeister et al., 2019a; Allen et al., 2020). An association between atmospheric circulation and mountain glaciers in the southern mid-latitudes has long been emphasized, for example by Mercer and Sutter (1982): "*The mountains in these latitudes lie across the prevailing westerly winds and, therefore, the surface temperature of the southern South Pacific Ocean has great influence of the extent of the glaciers.*" (p. 187). Twentieth-century glacier recession patterns in the Southern Alps were hypothesized by Harrington (1952) as resulting from a progressive net southward shift in the westerly wind flow, increasing the flux of warmer air masses across the Southern Alps. Reconstruction of New Zealand regional atmospheric circulation for the Late Holocene based on multiple precipitation- and temperature-sensitive proxies illustrates good correspondence between times of enhanced zonal atmospheric flow and Southern Alps glacier advances (Lorrey et al., 2008, 2014). These modern and Late Holocene analogues highlight the potential importance of oceanic and atmospheric circulation patterns to climate that may be relevant at decadal to orbital timescales.

3. Northern Hemisphere moraine records

We now turn our attention to physical evidence of glacier extent drawn from moraine chronologies from middle latitudes of the Northern Hemisphere. We focus on the European Alps because they

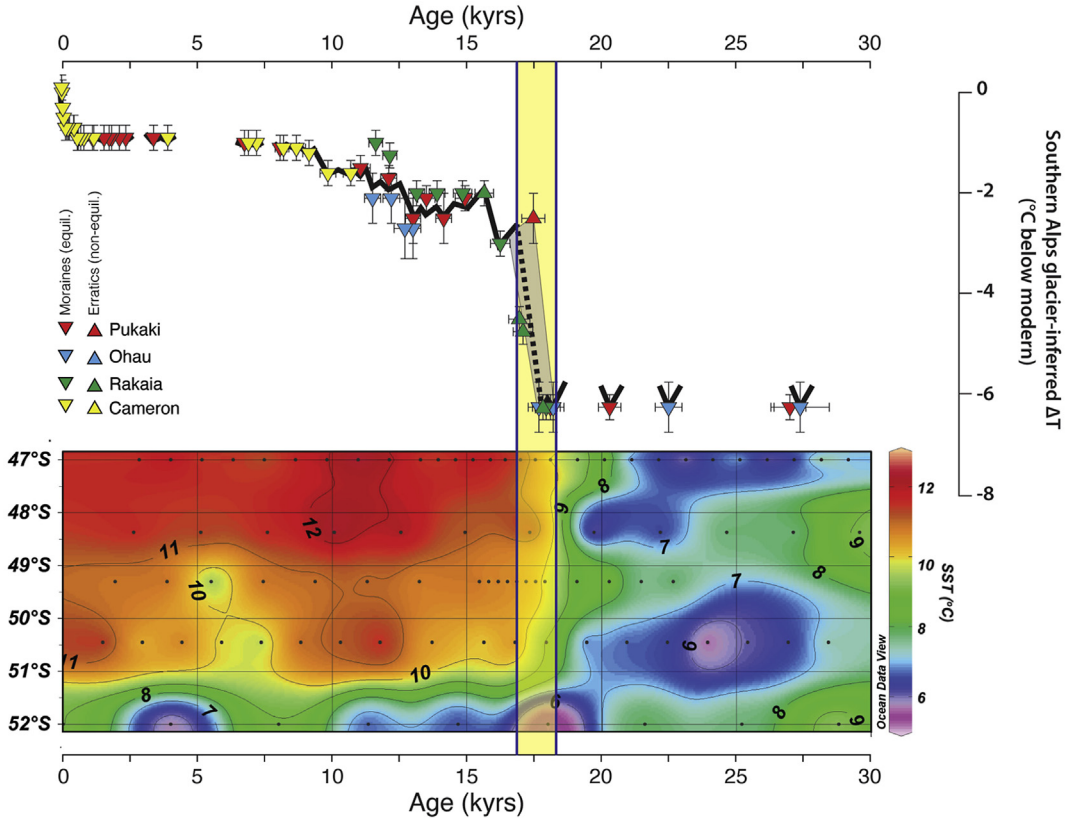

Fig. 6. Comparison of Southern Alps moraine ages and sea surface temperatures south of New Zealand. Top panel shows Southern Alps glacier-derived temperature reconstruction (details given in Fig. 4). Bottom panel is a latitudinal SST reconstruction from a suite of marine cores (Bostock et al., 2015; see Fig. 1). Yellow band corresponds to the period of greatest warming in both the surface ocean and the atmosphere, shortly after ~18 kyrs ago. (For interpretation of the references to color in this figure, the reader is referred to the Web version of this article.)

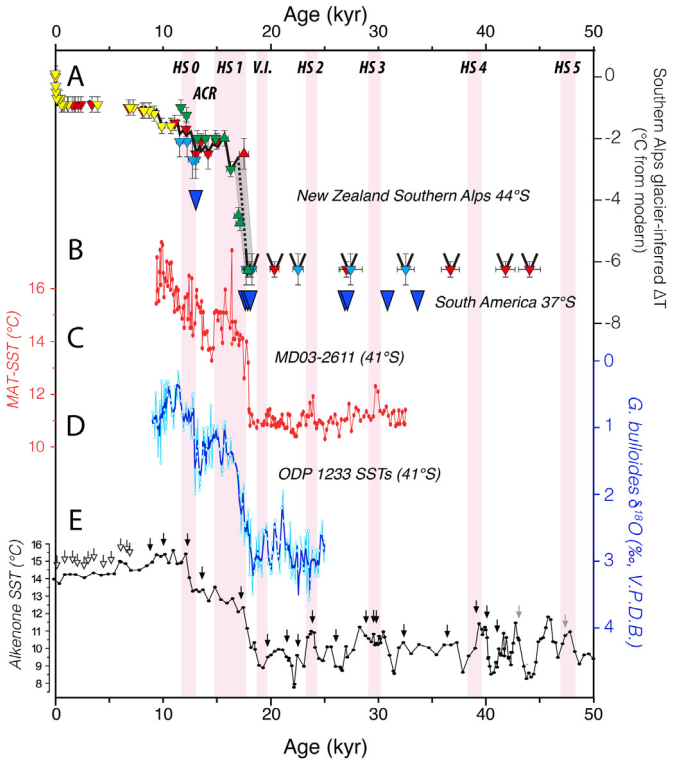

Fig. 7. Comparison of the timings of mountain-glacier maxima in the Southern Alps and the mid-latitude Chilean Andes, with SST variations near the STF. A) Southern Alps glacier-inferred temperatures (from Fig. 4). B) chronology of glacier advances in the Chilean Lake District (blue triangles (Denton et al., 1999b; Strelin et al., 2011)). C) Modern Analog Technique (MAT) SSTs from core MD03-2611, south of Australia (De Deckker et al., 2012). D) Planktonic $\delta^{18}O$ values, reflecting SSTs, from core ODP-1233 in the eastern South Pacific off the Chilean Lake District (Strelin et al., 2011). E) Alkenone-derived SSTs from core ODP-1233 (Kaiser et al., 2005). Downward-pointing arrows indicate positions of radiocarbon ages. Pink vertical bands correspond to Heinrich Stadials and the 'Varas Interstade' [V.I.; (Denton et al., 1999a)]. See Fig. 1 for core locations. (For interpretation of the references to color in this figure, the reader is referred to the Web version of this article.)

lie at a nearly antipodal location on the planet from the Southern Alps. Seasonally, the European Alps are under the influence of the boreal westerly winds, in a distal maritime setting downwind of the Atlantic Ocean (Florineth and Schlüchter, 2000). They thus have environmental similarities to the Southern Alps and southern Andes. Valley glaciers fed from mountain icefields terminated in piedmont lobes on the northern and southern borders of the European Alps between 23 and 25 kyrs ago, with relatively minor recession back to near the mountain front by ~18–19 kyrs ago (Ivy-Ochs, 2015; Wirsig et al., 2016a). As one example, the outboard components of the nested end-moraine system outboard of Lago di Garda, the largest moraine complex on the southern side of the European Alps, contain glacial landforms dating to shortly after 24.9 kyrs ago and again after 23 kyrs ago (Monegato et al., 2017). The last episode of the LGM (Manerba advance) produced a moraine belt on the inner rim of the Garda glacier trough and culminated at ~17.5 kyrs ago. This was followed closely by ice recession that is inferred to have been substantial. About 50 km farther west, the LGM moraine complex of the Oglio valley glacier shows a similar history, with an early LGM culmination shortly after 25.8 kyrs ago, and major ice withdrawal followed by the onset of post-glacial lacustrine sedimentation ~18 kyrs ago (Ravazzi et al., 2012). In the Austrian sector of the Alps, after loss of 80% of LGM ice volume, a relatively minor glacial resurgence (Gschnitz readvance) culminated at 16–17 kyrs ago (van Husen, 1997; Ivy-Ochs, 2015), by which time snowline had risen more than halfway from its LGM level to its interglacial position. Overall, much of the LGM glaciated area of the European Alps was free of ice by the end of Oldest Dryas (equivalent to HS1) (Ivy-Ochs, 2015), which in Switzerland is shown by the widespread distribution of sites with sediments that contain the characteristic Oldest Dryas pollen signal (Burga, 1988; Ivy-Ochs, 2015).

The recession is also tracked by ice downwasting from the LGM trim line in the central European Alps (Florineth and Schlüchter, 1998; Wirsig et al., 2016a, 2016b). ^{10}Be exposure dates of glacially-deposited boulders and glacially-molded bedrock surfaces from just below the LGM trim line show that the maximum ice surface near the Rhone ice-dispersal dome was achieved at close to 23 kyrs ago. Major lowering of the ice surface began no later than 17.7 ± 0.6 kyrs ago, which is similar in timing to surface lowering elsewhere in the interior European Alps (Wirsig et al., 2016a, 2016b). Overall, the interior European Alps glacier system underwent considerable downwasting early in HS1 prior to the Gschnitz resurgence.

There is also evidence for fluctuations of the European Ice Sheet during the LGM, and of sustained Northern Hemisphere ice-sheet recession following the LGM, during HS1 (e.g., Clark et al., 2012; Hughes et al., 2016; Margold et al., 2018; Dalton et al., 2020). There is a wealth of data on this topic, and we confine ourselves to highlighting two illustrative examples, one from Europe and one from North America. Proxies for meltwater discharge from the former Channel River in western Europe indicate increased meltwater flux from the European Ice Sheet during five intervals, at ~31-29 kyrs ago, ~26-23 kyrs ago, ~22 kyrs ago, ~20-19 kyrs ago, and between 18.0 ± 0.2 and 16.7 ± 0.2 kyrs ago (Toucanne et al., 2015; Boswell et al., 2019). The first four episodes represent melt episodes during the Last Glaciation, two of which occurred during HS2 and HS3, while the fourth suggests sustained deglacial melting during HS1. In northeastern North America, the southeastern margin of the Laurentide Ice Sheet adjacent to the North Atlantic Ocean in coastal Maine, had retreated more than 200 km from the LGM limit by 15.2 ± 0.7 kyrs ago (Koester et al., 2017).

4. North-south synthesis

Moraine chronologies from the mid-latitude Southern Hemisphere share important similarities with those from Europe and elsewhere in the Northern Hemisphere, in regard to fluctuations of ice-age glacier extents as well as the timing of the last glacial termination.

A prominent feature of southern mid-latitude Last Glaciation moraine records is repeated fluctuation of glacier extent, as represented for example in the Southern Alps by moraines formed by expanded glaciers at ~65 kyrs ago, ~44 kyrs ago, ~42 kyrs ago, ~37 kyrs ago, ~33-32 kyrs, ~27 kyrs ago, ~23-22 kyrs ago, ~20 kyrs ago, and ~18 kyrs ago. Glacier expansion is documented in the southern Andes at ~34 kyrs ago, ~31 kyrs ago, ~27 kyrs ago, and ~18 kyrs ago. European Alps records indicate major advances culminating at slightly younger than ~25 kyrs ago and slightly younger than ~23 kyrs ago. Enhanced melt episodes of the European Ice Sheet, suggesting boreal summer warming and concurrent ice recession, are indicated at ~31-29 kyrs ago, ~26-23 kyrs ago, ~22 kyrs ago, ~20-19 yrs ago. These chronologies indicate a commonality in lines of evidence for glacier advance/retreat in both hemispheres during an extended period of glacial-mode climate. The timing of glacial advance and moraine deposition in southern mid-latitudes was complemented by moraine construction and reduced meltwater fluxes in the northern mid-latitudes.

A widespread signal for mountain glacier systems in both hemispheres was the onset of sustained recession of ice beginning

~18 kyrs ago. For example, in the antipodal LGM ice fields of the Southern Alps and European Alps, post-glacial lakes are ponded behind the ~18-kyr-old moraine belts, such as Lake Ohau in the south and Lago di Garda in the north; sustained recession from those moraine belts was underway at about 17.7–17.5 kyrs ago (Putnam et al., 2013b; Ravazzi et al., 2014). This recession was accompanied by enhanced and sustained meltwater fluxes from the southern sector of the European Ice Sheet between ~18.0 and 16.7 kyrs ago, and retreat of the southeastern margin of the Laurentide Ice Sheet. Extensive glacier recession by ~17 kyrs ago was also registered at both ends of the American Cordillera, with coeval reduction of the western Cordilleran Ice Sheet in the north and the Patagonian Ice Sheet in the south. Altogether, these results indicate extensive ice withdrawal in both hemispheres beginning ~18 kyrs ago, suggesting that a fast and high-magnitude increase in atmospheric heat content initiated the close of the last ice age.

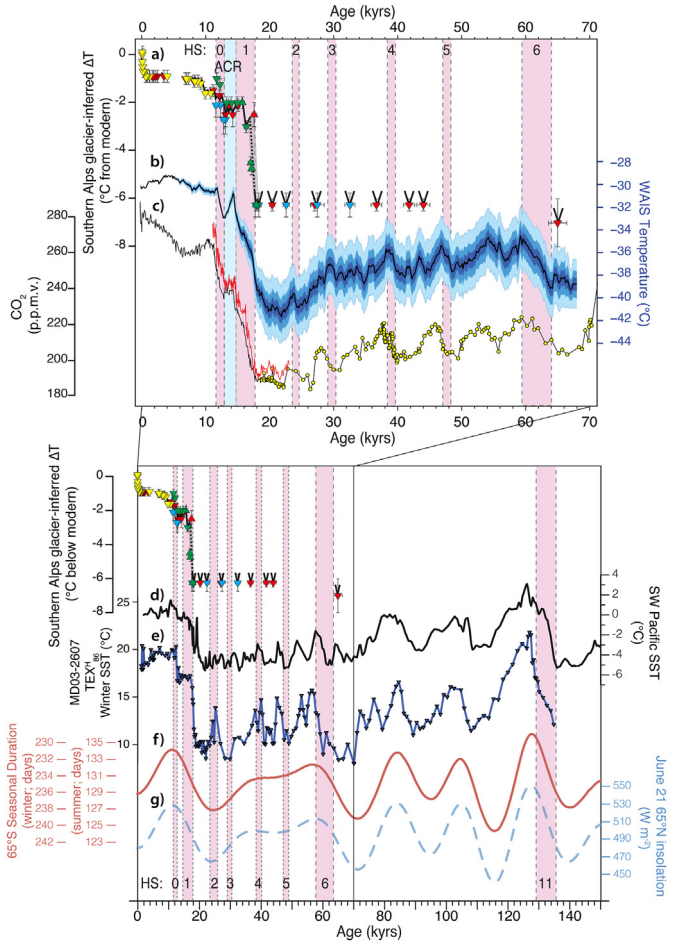

Fig. 8. Signatures of Southern Hemisphere climate variability. Note scale differences of upper and lower panels: a) Glacier-derived temperature reconstruction from the Southern Alps, 0–65 kyrs ago (Fig. 4); note its repetition in the lower panel. b) Antarctic ice core temperature (Buizert et al., 2015; Cuffey et al., 2016). c) Antarctic ice core CO_2 concentrations (Indermühle et al., 2000; Monnin et al., 2001; Ahn and Brook, 2008; Marcott et al., 2014). d) Sea-surface temperature stack derived from three marine sediment cores from the northern portion of the Southern Ocean, two from near New Zealand and one from the Indian sector (Barrows et al. 2007). e) TEX^{H}_{86} record of winter SSTs from core MD06-3207 offshore from southeastern Australia (Lopes dos Santos et al., 2013) (Fig. 1). f) Orbitally-controlled seasonal duration at 65°S [insolation threshold = 300 W/m^2; this threshold generally corresponds to midpoint insolation at 65°S latitude under modern climate, following Huybers (2006) and Huybers and Denton (2008)] and g) summer insolation intensity at 65°N.

The Southern Alps features a particularly well-resolved glacial landform record of the termination and subsequent events. The formation of late-glacial moraines in positions well up-valley of the moraine belts dated at ~18 kyrs ago took place in several events between ~16 kyrs ago and ~11.5 kyrs ago. We interpret the new locus of moraine formation in these valleys as evidence for a switch from glacial-mode climate to interglacial-mode climate (Figs. 4 and 5). Holocene-age moraines and modern glaciers, where still extant, lie a relatively short distance up-valley from the late-glacial moraine systems. Glaciological modeling indicates that the prevailing summertime climate was ~4–5 °C warmer during late-glacial than in the LGM, and only 1–2 °C colder than in the pre-industrial Holocene. Moraines in the European Alps occur in comparable geomorphic positions to those of the Southern Alps and illustrate a similarity of timing and magnitude of the switch between glacial and interglacial modes in both regions.

5. A southern modulator of global climate?

5.1. Framing the problem

A solution to the puzzles of ice-age climate must account for the interhemispheric symmetry of timing of ice-age mountain glacier fluctuations as well as the synchronous termination of the last ice age, registered widely in both hemispheres. Climate signatures in the South Pacific sector of the Southern Hemisphere over the last glacial cycle highlight, at a broad scale, similarities between Southern Ocean SST signatures and patterns of orbital variation (Fig. 8). Nevertheless, finer-scale (millennial) fluctuations, such as seen in the multiple glacial advances of the Southern Alps and southern Andes, do not accord with the pattern of orbital variation during the Last Glaciation (Mercer, 1984; Denton et al., 1999a; Doughty et al., 2015) (Fig. 8). We hypothesize that an explanation consistent with the physical evidence of ice-age glacier variability and deglaciation lies in changes in the latitude and intensity of Southern Hemisphere ocean and atmospheric circulation.

We see potential for such changes to account for not only millennial-scale fluctuations, but as a major contributor to climate shifts on the scale of a termination. Broecker and Denton (1989) highlighted major reconfiguration of circulation systems as a mechanism for changes in climate mode:

> "*glacial-to-interglacial transitions involve major reorganizations of the ocean-atmosphere system. Such reorganizations constitute jumps between stable modes of operation which cause changes in the greenhouse gas content and albedo of the atmosphere.*" (p. 2465).

We first set out a conceptual physical framework for the hypothesis and then test parts of it using an Earth System Model. We then discuss implications of the hypothesis for the interpretation of climate shifts inferred from moraine chronologies in both hemispheres.

5.2. Physical basis

The austral westerly winds and the coincident Southern Ocean surface isotherms constitute a fundamental feature of the climate system in the Southern Hemisphere. The position of the wind belt varies latitudinally on a seasonal basis, being more equatorward in the austral winter and more poleward in the austral summer. The latitudinal position of the westerlies covaries with wind intensity, with the westerlies strongest during summer when situated in a more poleward position (Russell et al., 2006a; Toggweiler et al., 2006; Toggweiler and Russell, 2008). Superimposed on

climatological variations driven by latitudinal temperature gradient changes, the intensity variations of the westerlies arise from conservation of angular momentum. Wind stress associated with the austral westerly belt fundamentally determines the Southern Ocean circulation and positions of frontal zones (Orsi et al., 1995).

Particularly important is the STF, which demarcates the zone of interaction between warm subtropical water and cool subantarctic water. During the global LGM the STF, the Subantarctic Front, and the Polar Front were equatorward of their present-day positions except where controlled by bathymetry (Sikes et al., 2009; Bostock et al., 2013, 2015). Adjacent to the Southern Alps, LGM SSTs were as much as 7 °C colder than today (Bostock et al., 2013), a value consistent with the temperatures necessary for Southern Alps glaciers to have maintained full-glacial positions. Close alignment between times of maximal extent of Southern Alps glaciers and episodes of coolest SST nearby (Pahnke et al., 2003; Doughty et al., 2015; Schaefer et al., 2015) implies millennial-scale co-variations in ocean temperature and glacier length. Recession of Southern Alps glaciers was coincident with a profound rise of SSTs south of New Zealand ~18 kyrs ago (Fig. 6). This is attributed to a poleward shift of the STF to a general position that has been maintained ever since (Bostock et al., 2015). South of Australia, a comparable warming of SSTs that occurred coevally at ~18 kyrs ago (Fig. 7) also implies poleward shift of the STF in that region (De Deckker et al., 2012). Overall, there appears to be a sound basis for linking glacier behavior in the Southern Alps with Southern Ocean sea-surface temperature gradients.

Central to the general circulation of the Southern Hemisphere are the geographic positions of the continental masses of Australia and Zealandia and the ocean currents surrounding them relative to the austral westerlies and the austral tropical easterlies. Mortimer et al. (2017) pointed out that the islands of New Zealand are a very small emergent part (5% by area) of the very large submerged continent of Zealandia. With extensive areas shallower than 1500 m depth, Zealandia exerts considerable influence on ocean currents (Bostock et al., 2013). For our discussion, the combined bathymetric and topographic relief of Australia and Zealandia is considered to approximate a mega continent (Australia/Zealandia). This mega continent is important because it intersects the Indo/Pacific Warm Pool (IPWP) and the Southern Ocean, as well as the tropical easterlies and the austral westerlies — no other continent plays host to such a critical climate crossroads.

To the northeast of Australia/Zealandia is the Pacific South Equatorial Current that flows west into the IPWP, with a limb feeding tropical water southwest into the Tasman Sea via the East Australian Current (EAC). Part of the EAC flow branches eastward around the northern tip of New Zealand as the Tasman Front, while part extends southwest as the EAC extension (EACE; Bostock et al., 2006). Surface water of the EACE eddies south towards Tasmania and merges into the STF, while part of the intermediate-depth EACE passes west around southern Australia as the Tasman Leakage (Speich et al., 2002, 2007; Ridgway and Dunn, 2007; Rosell-Fieschi et al., 2013; van Sebille et al., 2014). North of Australia/Zealandia is the Indonesian Throughflow conveying IPWP water west into the Indian Ocean and providing the most voluminous connection between Pacific and Indian ocean waters. To the south of Australia/Zealandia is the double-jetted Antarctic Circumpolar Current (ACC), while to the east the South Pacific gyre is the anticlockwise circulation of surface water between the South Equatorial Current and ACC. Near the southern margin of the mega continent is the equatorward edge of the modern austral westerlies. Southern Zealandia, the most poleward component of the mega continent, is like a 'boulder' in the stream of the circulating winds and ocean currents that link the global heat engine (the IPWP and tropical easterlies) with the ACC (Southern Ocean and austral westerlies).

5.3. Zealandia Switch hypothesis

Paleoclimatic records, taken together with a physical basis of modern climatology, indicate that the STF, and by implication the locus of the austral westerlies, maintained a relatively equatorward position during the Last Glaciation. We suggest that this configuration was a cornerstone of the glacial-mode climate condition as described by Broecker and Denton (1989), whereas the poleward shift of the circulation systems initiated at ~18 kyrs ago represented a reorganization to an interglacial mode of climate. We hypothesize that the unique configuration of continent-versus-ocean elements in the Australasian region introduces substantial consequences for subtropical oceanic circulation in the South Pacific, as shown in Fig. 9. We link the equatorward westerlies of glacial-mode climate with a latitudinally-restricted Indo-Pacific subtropical gyre system, whereas we link poleward westerlies of interglacial-mode climate with a latitudinally-expanded subtropical gyre system.

As noted by Lorrey and Bostock (2017), the restricted versus expanded gyre configurations are sufficiently different in relation to Australia/Zealandia bathymetry such that switching between them could produce fundamental and potentially far-reaching climate changes. The geographic setting of Australia/Zealandia brings into play the Island Rule (Godfrey, 1989) to connect latitudinal shifts of the austral westerlies with changes in tropical ocean circulation. By the Island Rule, an equatorward shift of the westerlies would decrease wind-driven eastward ocean flow along the southern margin of Australia/Zealandia, resulting in weakened westward ocean flow north of Australia/Zealandia (Russell et al., 2006a; Toggweiler et al., 2006; Toggweiler and Russell, 2008), including Indonesian Throughflow of tropical Pacific water into the Indian Ocean. Conversely, a poleward shift of the westerlies would strengthen ocean flow on the southern margin of Australia/Zealandia with an accompanying strengthening on the northern margin. Each case has differing consequences for the areal extent of warmest surface water in the IPWP, atmospheric convection, and production of water vapor. The intensity of the Indonesian Throughflow has consequences for flow patterns in the Indian Ocean, including westward Agulhas Leakage into the South Atlantic. An equatorward shift of the austral westerlies could simultaneously decrease Indonesian Throughflow and restrict Agulhas Leakage. The reverse could result from a poleward shift of the westerlies. In overall effect, the Island Rule would augment changes due to switches between latitudinally expanded and contracted gyres.

We suggest that the position of the austral westerlies relative to the Australia/Zealandia mega continent is important in explaining discrete shifts between glacial and interglacial modes of climate. At the heart of the mechanism is Zealandia and the way that it determines in large part whether the South Pacific subtropical gyre system was restricted or expanded (Fig. 9), and its effects on exchange of waters between the Southern Ocean and adjoining oceans. Thus we dub this hypothesis the Zealandia Switch. We view this switch as being a physical impediment to oceanic circulation, which is 'off' when circulation is in the equatorward position, and 'on' when in the poleward position. For example, at the change from glacial-to-interglacial mode ~18 kyrs ago the switch turned fully 'on'. We suggest that during the Last Glaciation when the Zealandia Switch was predominantly 'off', short-lived and/or small-amplitude latitudinal shifts of austral westerly circulation gave rise to millennial-scale climate fluctuations that are evident in the paleoclimate record.

5.4. Model simulation test of the conceptual framework

We developed a model simulation to evaluate the consequences

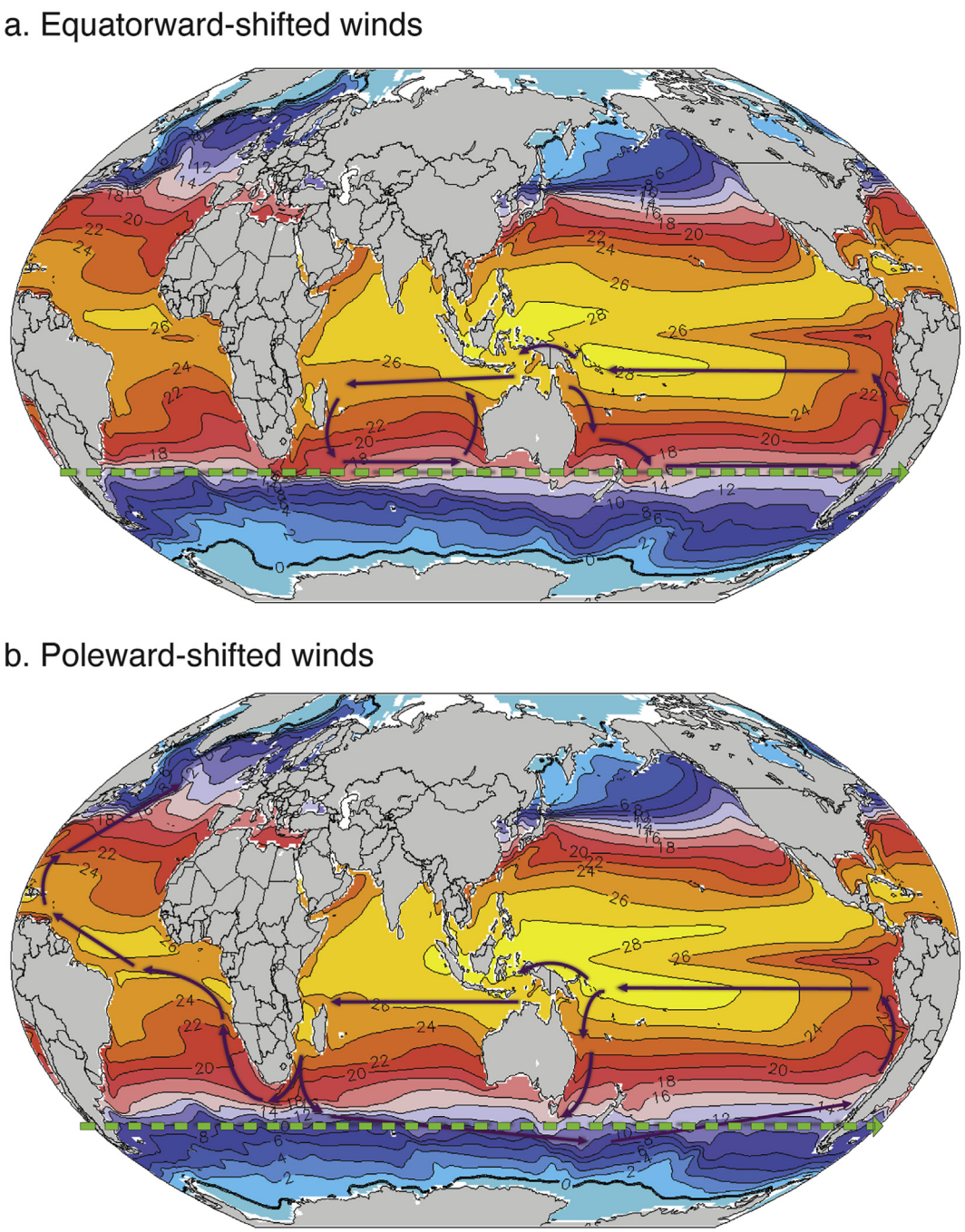

Fig. 9. Schematic diagram depicting the latitudinally contracted (panel a; equatorward winds) and expanded (panel b; poleward winds) gyres that reflect the operation of the Zealandia Switch. Green dashed lines represent the latitude of the mean locus of the austral westerlies and solid dark purple arrows represent the approximate loci of prominent near-surface ocean currents. The colors represent the near-surface ocean temperatures shown and described in Fig. 11. (For interpretation of the references to color in this figure, the reader is referred to the Web version of this article.)

of different latitudinal positions of the austral westerly circulation. This experiment was designed to determine whether shifts of the austral westerlies, taken in isolation, could produce the conditions needed for global-scale temperature change. To ensure that we used the best-resolved boundary conditions for the model, we employed an initial (control) model based on pre-industrial modern climate. We then compared that to a model in which we applied a uniform wind-stress perturbation (perturbation run) that would mimic the effects of poleward-shifted austral westerlies. The modeling is not intended to be a recreation of any specific climate scenario, but rather focuses on assessing the sensitivity and effects of latitudinal wind shifts.

The modeling experiment was carried out in an ensemble of 30 simulations using a state-of-the-art coupled Earth System Model (ESM) from NOAA's Geophysical Fluid Dynamics Laboratory, ESM2M (Dunne et al., 2012, 2013). We used ESM2M, because it affords a reasonable representation of the modern wind systems (Russell et al., 2006a, 2006b). The control is based on the standard CMIP DECK preindustrial control simulation using fixed preindustrial atmospheric conditions. As in CMIP5 simulations, the control

model has an initial wind-stress maximum too far equatorward (Bracegirdle et al., 2013). This means that the so-called preindustrial model has the austral westerlies in a position that may resemble that inferred here for glacial-mode climate conditions.

In the perturbation run, we applied a momentum-flux adjustment to approximate poleward-intensified westerlies computed by the ESM (Fig. 10), employing the methodology used in Delworth and Zheng (2008) and consistent with the protocol applied by the Southern Ocean Model Intercomparison Project (Bronselaer et al., 2017). The wind perturbations have a defined latitudinal profile and branch from the CMIP DECK preindustrial control simulations. Our experiment executed a 200-year integration with the anomalous wind-stress forcing added to the internally-generated wind stress uniformly at all longitudes (Fig. 10). Other than the application of a wind stress perturbation, no other parameter was changed. This wind perturbation simulation is a significant component of the ongoing Southern Ocean Model Intercomparison Project (Bronselaer et al., 2017). The results of that experiment now have been replicated in a 20-member ensemble and are considered to be robust for this model. A strong poleward increase in the wind stress allows a direct assessment of the ability of wind forcing both to mix surface properties downward in the water column and to bring interior properties to the surface. The poleward wind stress also stimulates upwelling of Circumpolar Deep Water alongside Antarctica.

The perturbation run simulation of poleward westerlies shows a switch from a restricted to an expanded subtropical gyre. There is general oceanic warming in both hemispheres, with strong warming being registered across much of the Southern Ocean, in the Indo-Pacific region, and in particular in the North Atlantic region (Figs. 10 and 11). Indonesian Throughflow is increased due to a change in the surface height of western tropical Pacific water, along with enhanced southward flow of tropical water in the EACE at the expense of flow along the Tasman Front (Fig. 11). The perturbation run shows a wide spread of warm water across the tropical ocean (Fig. 12). Warm surface water is also distributed to the Southern Ocean via the EACE, while warm intermediate-depth water is distributed westward into the southern Indian Ocean via the

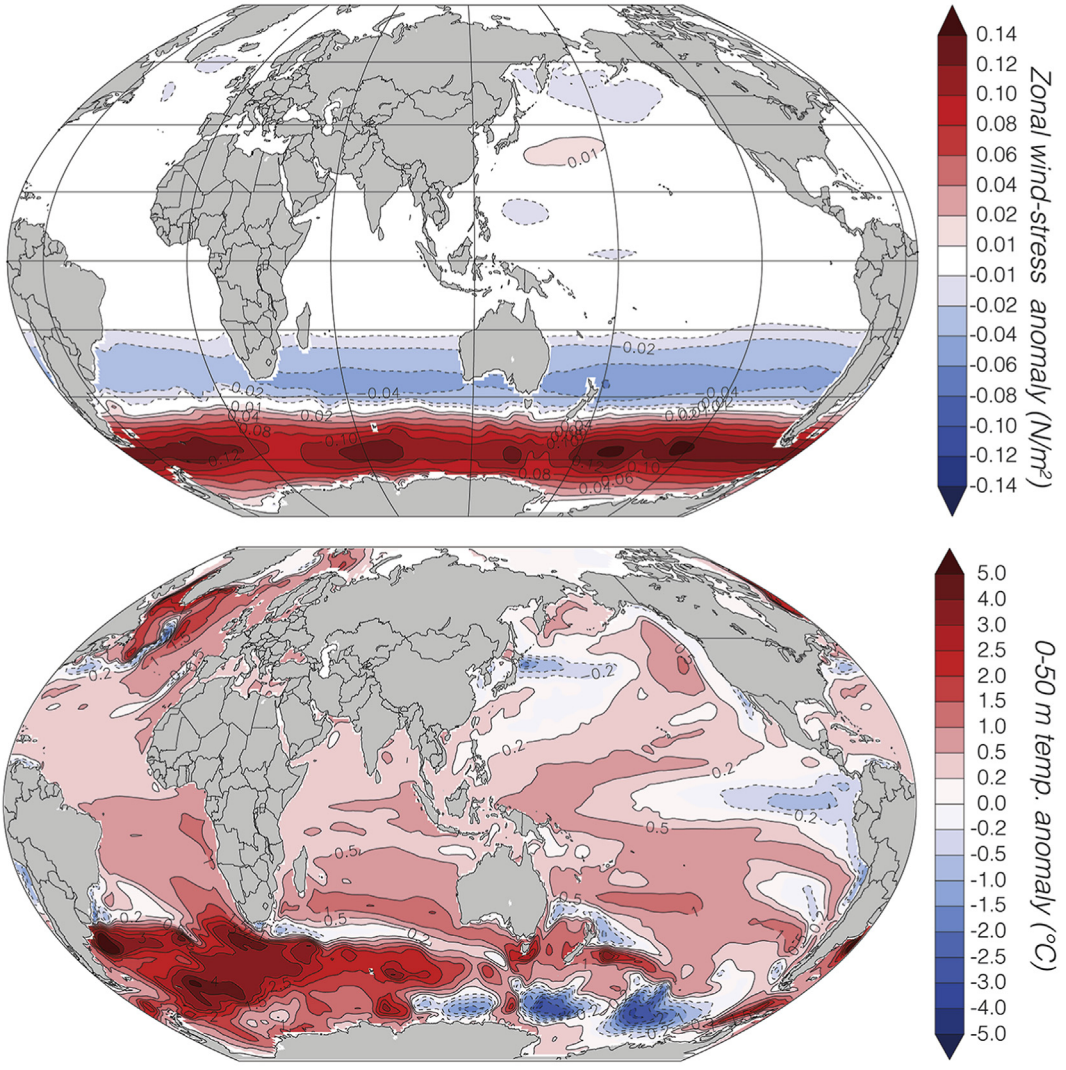

Fig. 10. A model simulation of the effect of poleward-shifted austral westerlies. Top panel: Zonal wind-stress perturbation (i.e., momentum-flux adjustment) imposed upon the pre-industrial climate system to simulate the global impacts of a shift of the austral westerlies. Color scale represents the difference in zonal wind stress between simulations representing the pre-industrial equatorward wind position and the poleward wind-anomaly position. Bottom panel: Surface temperature anomaly of the global ocean (0–50 m) in response to the imposition of poleward-shifted austral westerlies relative to the preindustrial control simulation, integrated over 200 years. The bulk of the upper ocean in both hemispheres warmed in response to the poleward wind shift, with notably strong responses in the Indian and Atlantic sectors of the Southern Ocean and in the North Atlantic. (For interpretation of the references to color in this figure, the reader is referred to the Web version of this article.)

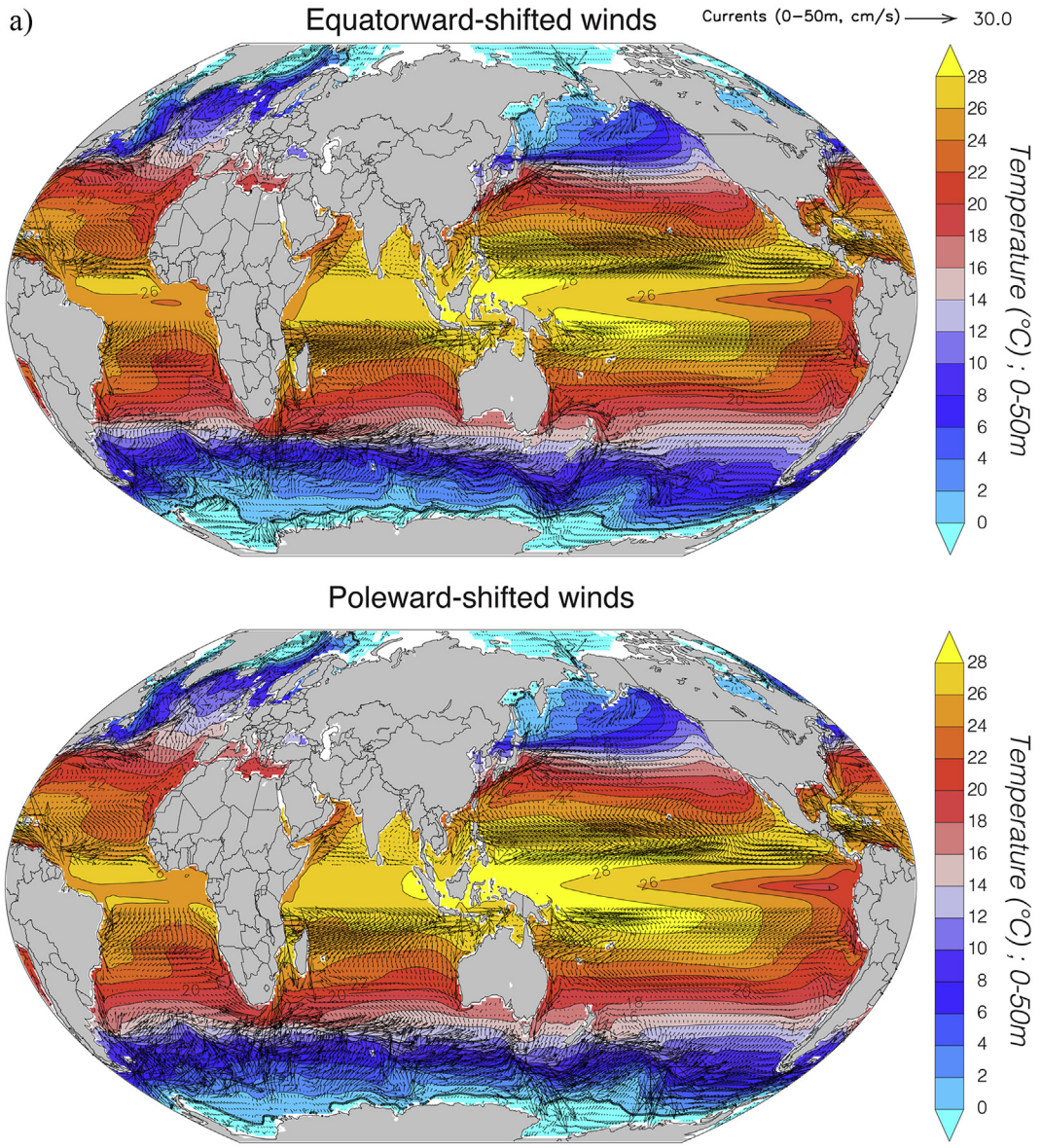

Fig. 11. a. Global near-surface ocean currents and SSTs under an equatorward versus poleward westerly wind regime, integrated over 200 years. Near-surface currents and ocean temperatures, integrated from 0 to 50 m water depth, are represented as vectors and colors, respectively. Note the response in flow through the Tasman Front and Agulhas Leakage in response to a transposition of the latitude of the westerlies. Fig. 11b. Detail of model results for the Australasian region, illustrating that with winds in a poleward position, the East Australian Current extends south to the Southern Ocean, at the expense of eastward flow along the Tasman Front north of New Zealand. The bottom panel is a detailed view of the near-surface ocean temperature anomaly model shown in Fig. 10. (For interpretation of the references to color in this figure, the reader is referred to the Web version of this article.)

Tasman Leakage. The STF also exhibits a hemisphere-wide concentric poleward contraction (Fig. 11). Attendant increased Agulhas Leakage (Fig. 11) is at least partly responsible for warming in the tropical and northern Atlantic, reflecting net increase in northward oceanic heat transport. South of Australia, the poleward contraction permits eastward flow of surface water in the Leeuwin Current (Fig. 11).

About 80% of the poleward heat transport today is from atmospheric transport of tropical water vapor (Fasullo and Trenberth, 2008). A consequence of a poleward shift of the austral circulation on the subtropical gyre system, as indicated in the perturbation run, would be broadening of the area subject to tropical/subtropical atmospheric convection, thereby increasing the global water vapor feedbacks without requiring a coincident increase in atmospheric CO_2.

5.5. The last glacial termination in the context of the Zealandia Switch hypothesis

Prior to the termination, the Southern Ocean was in an expanded glacial-mode state, and cold conditions prevailed across nearby landmasses, with fully extended glaciers in the Southern Alps and mid-latitude Andes. Beginning ~18-kyrs ago, the following changes took place. The Southern Ocean contracted rapidly. The westerly wind system and STF shifted poleward. The subtropical gyre systems switched from a latitudinally-confined to a latitudinally-expanded configuration. Strengthened flow and southward extension of the Leeuwin Current and EACE allowed subtropical water to circulate around the southern margins of Australia and New Zealand (De Deckker et al., 2012; Bostock et al., 2015) (Figs. 6 and 7). The enhanced flow of warm water into the

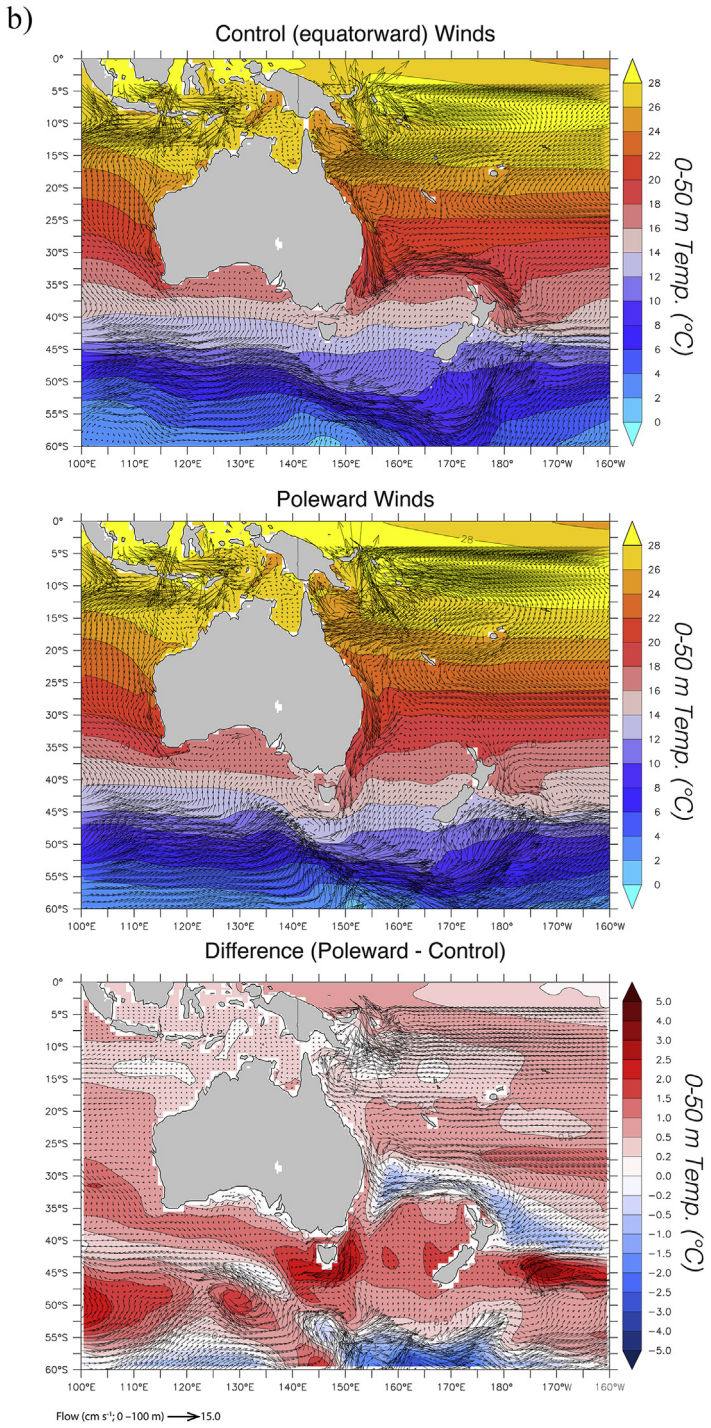

Fig. 11. (*continued*).

central and southern Tasman Sea facilitated the advection of warmer atmospheric temperatures across New Zealand via prevailing westerlies (Lorrey et al., 2020), thus causing glacier retreat in the Southern Alps. A coincident warming of surface ocean water off the western coast of southern South America, illustrated in Fig. 7, accompanied recession of Andean glacier lobes in mid-latitude South America. The similarity of these climate changes across the southern Pacific Ocean is consistent with a zonally symmetrical poleward shift of the austral wind system during deglaciation. Such a poleward shift over the Southern Ocean not only would have affected the tropical/subtropical circulation, but also would have enhanced upwelling of abyssal water south of the Polar Front. This upwelling would have released CO_2 from the deep ocean into the atmosphere (Figs. 13 and 14), while at the same time warming the surface of the Southern Ocean because upwelled water was warmer than surface water (Anderson et al., 2009; Bard and Rickaby, 2009; Biastoch et al., 2009; Lamy et al., 2010; Lee et al., 2011; McGlone et al., 2010; Putnam et al., 2010a; Skinner et al., 2010; He et al., 2013; Kohfeld et al., 2013; Sime et al., 2013; Allen et al., 2015, 2020; Gottschalk et al., 2016; Jaccard et al., 2016; Pedro et al., 2016; Saunders et al., 2018; Fogwill et al., 2020).

Our modeling results (Fig. 10) show that shifts of the austral

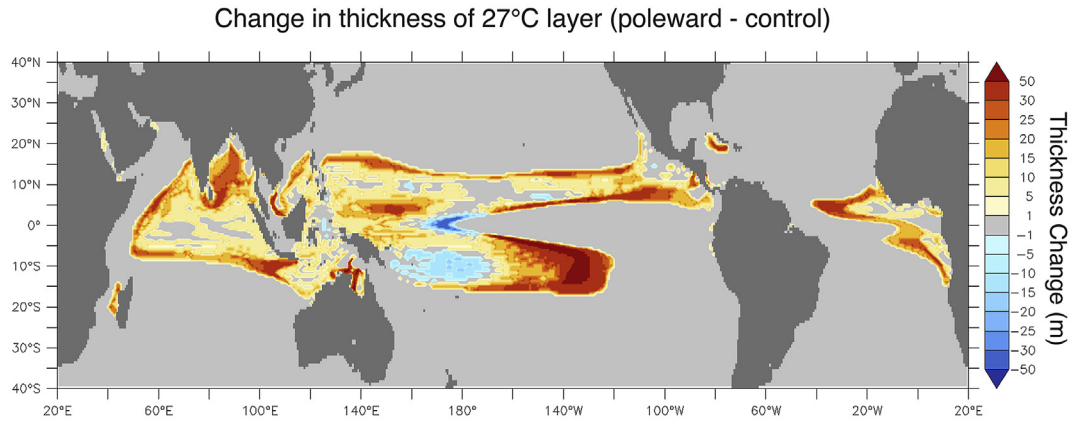

Fig. 12. Tropical Pacific response to poleward shift of the austral westerlies, integrated over 200 years. Map of the warm water depth anomaly, expressed as the depth of the 27 °C layer (approximating the thickness of the layer). Warm tropical waters expand into the Pacific subtropics and Indian Ocean in response to the poleward wind shift.

westerlies have global consequences, including in the North Atlantic region, suggesting an explanation for the complementary glacier changes in the two hemispheres described earlier. For example, a decisive poleward shift of the austral westerlies could have initiated global warming during HS1 by increasing the transport of latent heat into both hemispheres in the form of atmospheric water vapor sourced from an enlarged subtropical gyre system with its warmer SSTs. In this context, the increasing temperatures registered by various proxies across the Southern Ocean and Antarctica represented the globally extensive warming resulting from the Zealandia Switch turning on, while HS1 is viewed as a powerful interregional northern climatic response to that warming.

During the LGM, the North Atlantic Ocean overturning circulation center lay between the North American and Eurasian continents. The large ice sheets on those continents drained meltwater and calved icebergs into the North Atlantic. The HS1 summer warming registered by ice retreat in the European Alps, the southeastern Laurentide Ice Sheet, and the southern European Ice Sheet would have increased discharge into the North Atlantic of meltwater and icebergs. Freshening and stratification of the North Atlantic resulted in the formation of extensive winter sea ice. The overall result in northern latitudes would have been extreme seasonality that featured severe winter cold triggered by the warm summers that produced the enhanced meltwater and iceberg discharge into the North Atlantic. The accentuated boreal winter interhemispheric thermal contrast produced by extreme Northern Hemisphere seasonality is consistent with a net southward shift of the Intertropical Convergence Zone (ITCZ) and associated monsoon systems (Denton et al., 2010; Broecker and Putnam, 2013; Putnam and Broecker, 2017). Northern Hemisphere monsoons weakened, for example in Asia (Dykoski et al., 2005; Wang et al., 2008; Cheng et al., 2009). Low-latitude austral summer monsoons strengthened, for example in South America (Wang et al., 2004, 2007; Kanner et al., 2012; Martin et al., 2020) and Australasia (Ayliffe et al., 2013). Overall these adjustments reflected changes in the interhemispheric temperature contrast (Broccoli et al., 2006) produced by differing hemispheric seasonality responses to global warming during the last glacial termination.

In summary, we suggest that northern mid-latitude ice bodies reacted sensitively to warmer boreal summer temperatures during HS1 because surface ice ablation was dominated by summer melting, but the ice bodies were relatively insensitive to colder winters. In contrast, the climate record interpreted from Greenland ice cores was dominated by especially cold winters caused by the stratification and sea-ice cover on the adjacent North Atlantic, which in turn depended on summer surface melting of adjacent ice bodies. By promoting North Atlantic stratification, surface melting of ice sheets was likely augmented by increased subsurface melting at ice-sheet grounding lines due to ocean warming (e.g., Marcott et al., 2011; Bronselaer et al., 2018; Haumann et al., 2020). The winter atmospheric cooling induced by the spread of sea ice on the meltwater-freshened surface of the North Atlantic far outweighed the more modestly causative summer warming (Isarin et al., 1998; Isarin and Renssen, 1999; Denton et al., 2005), which therefore is nearly obscured in the Greenland ice-core record. The hydrological response to the strong boreal winter signal included net southward latitudinal shifts of monsoonal rain belts and the ITCZ (Broecker and Putnam, 2013; Putnam and Broecker, 2017), as well as changes in the area and surface elevations of the pluvial lakes in the western United States (Broecker and Putnam, 2012; Munroe and Laabs, 2013; Putnam, 2015). The results from our simulations of poleward-intensified westerlies and the physical evidence from moraine chronologies suggest that the mechanism underpinning these boreal winter changes was a latitudinal shift of the austral westerlies that produced a powerful tropical and subtropical response, warming the globe and melting ice bodies in both hemispheres.

6. Discussion

There are several implications of the Zealandia Switch hypothesis for climate change, in addition to those noted above.

First, Mercer's Paradox remains unresolved more than three decades after the problem was framed by Mercer (1984). The chronologies of southern moraines set out here underscore Mercer's (1984) doubt as to whether the Murphy/Milankovitch summer insolation mechanism acting on ice-sheet mass balance was truly the major driver of global glaciation. Instead of providing support for a summer-intensity driver that was out of phase in the two hemispheres, the moraine chronologies point to a globally-synchronous LGM and last deglaciation, a situation that also applies to the longer-term oscillations shown in Fig. 15 (Huybers, 2011). The problem is accentuated by the finding that during the Last Glaciation, mid-latitude icefields in the Andes and the Southern Alps did not show an identifiable response to orbital-scale variations in local summer insolation intensity (Mercer, 1984; Denton et al., 1999; Putnam et al., 2013b; Doughty et al., 2015; Strand et al., 2019). It is particularly noteworthy that the termination of the last glacial cycle in southern mid-latitudes occurred

during a phase of falling, not rising, local summer insolation intensity.

The overall findings from moraine chronologies highlight the problem of why glaciation and deglaciation had an interhemispheric rhythm if summer insolation intensity, which was antiphased between the hemispheres, truly controlled glaciation (Huybers, 2009), in other words, Mercer's Paradox. To circumvent this problem we suggest that, instead of being focused on ice sheets, the primary orbital linkage to ice-age climate was the effect of seasonal variations in solar energy on changes in the latitude and strength of the austral westerlies that affected the tropical Pacific Ocean and hence global climate through the Zealandia Switch hypothesis. Such a primary linkage not only addresses Mercer's Paradox, but it also recognizes the Cane (1998) suggestion of a leading role for the tropical Pacific Ocean in ice-age climate change. At the same time, the behavior of the austral westerlies may tie the pacing of changes in the tropical Pacific into a high southern latitude orbital signal whose signature mirrored that in high northern latitudes.

The principal orbital linkage to the southern westerlies may have been variations in the duration of mid-and-high-latitude austral summer/winter seasons (Huybers and Denton, 2008). The signature of southern seasonal duration mirrors that of mid-summer boreal insolation intensity (Fig. 8). Thus orbitally-driven changes in southern seasonal duration, encapsulating the joint effects of summer and winter season length changes, may have paced the seasonal cycle of the Southern Hemisphere westerly wind field with a pulsebeat similar to that of 65°N midsummer insolation. But there may also be other relevant effects of orbital variation on components of the southern climate system that await identification and quantification. The mechanisms outlined for the Zealandia Switch hypothesis afford ways of globalizing a southern-initiated warming through atmospheric and oceanic circulation, especially via the tropical Indo/Pacific Warm Pool and the Agulhas Leakage (Turney and Jones, 2010).

The hypothesized Zealandia Switch mechanism for a termination involves similar elements employed in the Denton et al. (2010) hypothesis. A major difference is that Denton et al. (2010) utilized the classic Milankovitch orbital summer forcing on northern ice sheets to initiate the last glacial termination, whereas here we suggest an alternative through globalization of orbitally-induced southern warming. Nevertheless, the extensive northern mid-latitude continental ice sheets remained important because their large size and low surface gradients made their ablation/accumulation areas sensitive to temperature change. Atmospheric warming would have markedly increased ablation areas and impacted mass balance. Postulated knock-on effects included increased meltwater flux into the North Atlantic, unloading and destabilizing of marine-based sectors of the ice sheets, and resulting enhanced iceberg production (Bard et al., 2000; Barker et al., 2015). Consequent North Atlantic stadial conditions were marked by extreme seasonality with hyper-cold winters. Altered (i.e., flattened) interhemispheric temperature gradients provide a plausible explanation for net southward shift of the ITCZ that characterized northern stadials. Whether the overall ITCZ position was drawn south by southern-initiated warming or pushed south by the resulting northern cold stadial is an open question that may be resolvable from detailed chronologies of ITCZ-related proxies.

Abrupt temperature shifts indicated in Greenland ice core records compared to more gradual temperature changes registered in Antarctic ice core records could be taken to indicate that the changes originated proximally to Greenland, with muted distal signatures in the south. However, the environmental setting of each of those ice core records is important. Taking the example of a poleward shift of the austral westerlies, we envision a progressive warming as atmospheric and oceanic systems adjusted, with the change globalized over years to decades. For temperate ice bodies sensitive to seasonal summer ablation, a sustained shift to warmer summers would likely be expressed almost immediately by increased meltwater. By the Zealandia Switch hypothesis, global warming sourced from the Southern Hemisphere led to enhanced northern ice-sheet ablation with rapidly increased meltwater flux into the North Atlantic, causing extensive winter freezing that was registered by isotopic signatures in Greenland ice. By that scenario, it seems that an onset of warming would have been registered abruptly in Greenland. But counterintuitively, because of extreme seasonality, ice-core proxies for mean-annual temperature may be more appropriately interpreted as predominantly reflecting the signature of very cold winters that overwhelmed signatures of warmer summers (Denton et al., 2005; Buizert et al., 2014).

The Zealandia Switch mechanism is suggested to operate on both orbital and millennial time scales. Poleward shifts of the southern circulation system would have stimulated global warming, and equatorward shifts, global cooling. While acknowledging that insolation intensity/seasonal duration probably has had some influence on ice bodies via sensible heat, we suggest it was comparatively minor. Our alternative perspective from the Zealandia Switch hypothesis is that the underlying control of global ice volume arises from orbital forcing acting on the Southern Hemisphere, and the resulting condition of the Southern Ocean. In that view, the climatic state of the Southern Ocean may be globalized via atmospheric and oceanic processes and thereby influence the size of the northern continental ice sheets. In sum, we suggest that the Zealandia Switch mechanism affords a functional explanation for the global rhythm of orbital-scale ice-age climate oscillations. Rather than originating from the influence of warm summers on ice-sheet mass balance (Murphy, 1869; Milankovitch, 1941), the primary orbital pacing of global ice-age climate in the Zealandia Switch mechanism emerges from variations acting on the Southern Hemisphere oceanic and atmospheric circulation.

Second, the Zealandia Switch mechanism may help explain the atmospheric CO_2 signal of the last glacial cycle shown in Figs. 13 and 14. The southern-latitude moraine records suggest that the austral westerlies commonly occupied equatorward positions as the last glacial cycle progressed, for example during MIS 4, MIS 2, and parts

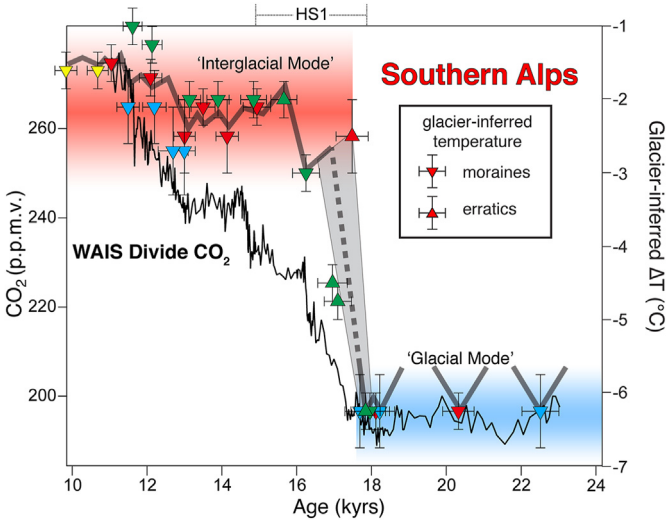

Fig. 13. Comparison of Southern Alps glacier-derived temperatures with the rise of atmospheric CO_2 during the last termination. Glacier-derived temperatures and related symbols are the same as in Fig. 4. The atmosphere achieved near-interglacial temperatures by as early as ~17 kyrs ago, whereas CO_2 had only risen by a few ppm.

of MIS 3. As equatorward-shifted westerlies became less aligned with the Antarctic Circumpolar current, the exchange of surface and deep water in southern latitudes could have weakened, leading to the buildup of a CO_2 capacitor in the deep ocean due to reduced mixing. Tapping of this ocean capacitor by Southern Ocean upwelling caused by poleward-shifted austral winds could have produced much of the rise of atmospheric CO_2 at the end of the last ice age. As well as contributing to global warming, the sustained deglacial rise in atmospheric CO_2 shown in Fig. 14 could have held the climate system in an interglacial mode when concentrations exceeded 230 ppm (Toggweiler et al., 2006), countering any tendency for a return to a glacial regime. We note that this threshold was breached only during HS1 and not during previous Heinrich stadials (Fig. 14), and also that this CO_2 threshold had been achieved early enough to hold the system in an interglacial regime during the late-glacial ice readvances shown in Figs. 3 and 4. Overall, we suggest that a central role of atmospheric CO_2 is a tendency to hold the austral westerlies, and thus global ice-age climate, into a glacial or an interglacial mode. In such a case a major switch of the austral westerlies between equatorward or poleward modes occurs only when orbital forcing overcomes the tendency of atmospheric CO_2 to maintain a particular mode.

Third, the orbital rhythm varies about a mean state, but Late Quaternary glacial cycles had an asymmetric 'saw-tooth' climatic signature. We suggest this may reflect internal resilience within Earth's climate system (Schaefer et al., 2015). For example, whereas MIS 3 saw a return of intermediate-value orbital insolation/seasonal duration parameters, southern mid-latitude mountain glaciers re-advanced several times to full-glacial extent. Net global ice volume, expressed by sea level, continued to increase during this time (Fig. 15). Relatively low atmospheric CO_2 may have afforded conditioning against a mode shift out of glacial climate during MIS 3, but the Southern Ocean also may have had a role. We suggest that once the Southern Ocean is stratified, it may be difficult for it to break out of that condition. The prominent millennial-scale climate fluctuations of the Last Glaciation and deglaciation, by the Zealandia Switch hypothesis, arose from net latitudinal shifts of the austral westerlies. Each poleward shift caused southern warming which by Zealandia Switch mechanisms was globalized to induce northern ice-sheet melt and disintegration, producing the strong seasonality signature of a northern Heinrich stadial. When such shifts did not coincide with sustained strong orbital conditioning, they failed to take hold and a global climate mode shift did not occur (i.e., resulting in a 'failed termination'). Instead, climate reverted back toward glacial conditions and the climatic descent continued towards the global LGM, and ongoing loading of the CO_2 ocean capacitor. About 18 kyrs ago, a poleward shift of the austral westerlies coincided with ideal orbital circumstances and maximal northern ice sheets. That change produced a full termination via a rapid shift to interglacial-mode climate that, over the course of several millennia, was locked in through the deglacial CO_2 rise.

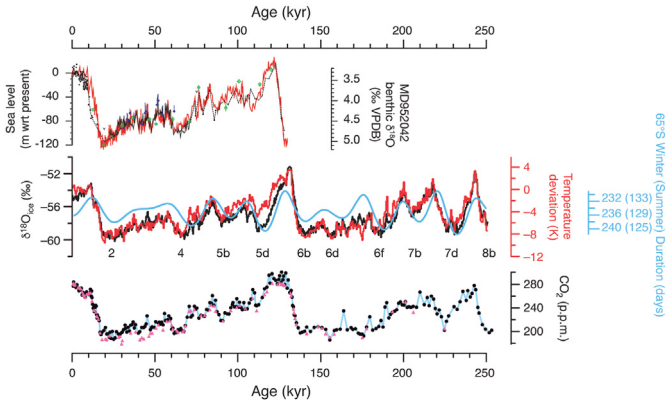

Fig. 15. Orbital signals compared with sea level and ice-core data. Top: Red Sea sea-level reconstruction (Siddall et al., 2003). Middle: Dome Fuji ice-core d^{18}O (black) and air-temperature reconstruction (red) (Kawamura et al., 2007) compared with seasonal duration curve (blue; insolation threshold = 300 W/m^2). Bottom: Dome Fuji CO_2 record (Kawamura et al., 2007). (For interpretation of the references to color in this figure, the reader is referred to the Web version of this article.)

Fourth, and perhaps most significant, the Zealandia Switch mechanisms may be operative in today's warming world and could potentially induce a new 'super interglacial' climate mode (Turney and Jones, 2010). This suggestion is rooted in the observation that several of the processes inferred to have spurred the glacial/interglacial climate switch in the Southern Alps and globally have renewed their operation in recent decades. The austral westerlies have progressively shifted poleward and strengthened, which has been partially attributed to increased atmospheric CO_2 (Gillett and Thompson, 2003). The EACE has strengthened and increased the delivery of warm water to the southwestern Tasman Sea (Cai et al., 2005; Ridgway, 2007; Ridgway and Dunn, 2007; Hill et al., 2008), while Southern Alps modern glaciers have lost considerable

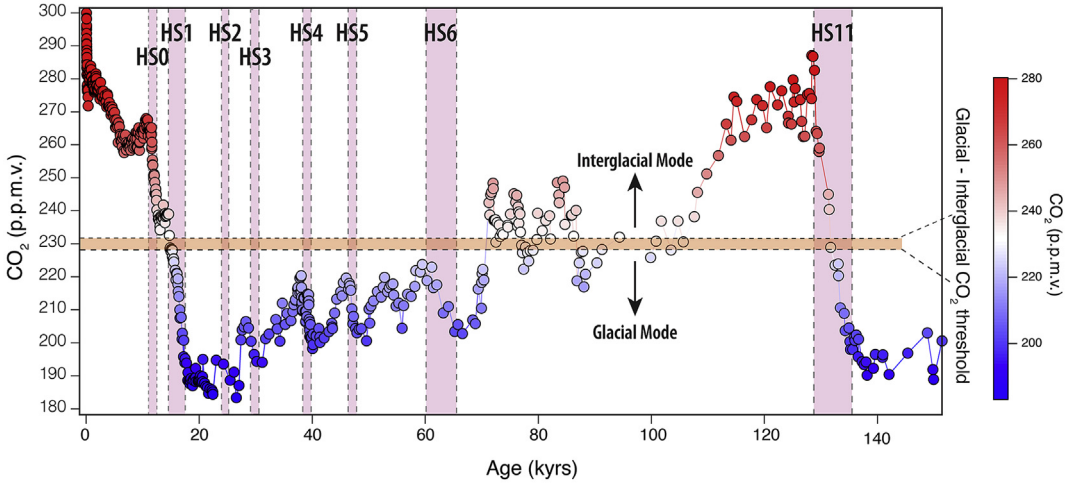

Fig. 14. Glacial-interglacial CO_2 threshold. Antarctic ice-core CO_2 compilation is same as that from Fig. 8. Orange horizontal band depicts CO_2 threshold, centered around ~230 ppm. (For interpretation of the references to color in this figure, the reader is referred to the Web version of this article.)

volume (Chinn, 2012). Recent marine heatwaves in the Tasman Sea have led to strong warming in New Zealand (Oliver et al., 2017; NIWA, 2018; Oliver et al., 2018). Further investigation into the role of the austral westerlies in climate change should afford better insight into how global climate is likely to respond to the ongoing rise of atmospheric CO_2.

Finally, the Zealandia Switch mechanism has potentially far-reaching implications for understanding past and future climate shifts. Thorough testing is needed using a wide range of proxy data, models and accounting for seasonal sensitivities. What remains clear, however, is that mountain glacier systems are an invaluable source of information because they respond rapidly to shifts in climate. During glaciations, mountain glaciers formed in many locations scattered across tropical and northern latitudes. Dating of moraines in a consistent way affords a good opportunity to test whether the climate mechanisms espoused here for the mid-latitude Southern Hemisphere had globally-extensive reach.

7. Conclusion

Three decades ago Broecker and Denton (1989, p. 2465) pointed out a key Quaternary science problem that was still unresolved, namely that the linkage between orbital cycles and ice-age climate awaits satisfactory explanation. *"Although we are convinced that the Earth's climate responds to orbital cycles in some fashion, we reject the view of a direct linkage between seasonality and ice-sheet size with consequent changes in climate of distant regions. Such a linkage cannot explain synchronous climate changes of similar severity in both polar hemispheres. Also, it cannot account for the rapidity of the transition from full glacial toward full interglacial conditions. If glacial climates are driven by changes in seasonality, then another linkage must exist."*

The mapping and dating of mid-latitude Southern Hemisphere mountain-glacier moraines leads us to the view that the latitude and strength of the austral westerlies, and their effect on the tropical/subtropical ocean, particularly in the region spanning the Indo-Pacific Warm Pool and Tasman Sea through to the Southern Ocean, provides an explanation for driving orbital-scale global shifts between glacial and interglacial climatic modes, via the Zealandia Switch mechanism. We suggest that this mechanism is the missing linkage highlighted by Broecker and Denton (1989). The same mechanism may have been the source of millennial-scale climate shifts that were a prominent feature of glacial-mode climate. Such behavior of the ocean-atmosphere system may be operative in today's warming world, introducing a distinctly non-linear mechanism for accelerating global warming due to atmospheric CO_2 rise.

Author statement

George Denton: Conceptualization; Methodology; Validation; Investigation; Writing – Original Draft; Writing – Review & Editing; Supervision; Project Administration; Funding acquisition. Aaron Putnam: Conceptualization; Methodology; Validation; Investigation; Writing – Original Draft; Writing – Review & Editing; Visualization; Project Administration; Funding acquisition. Joellen Russell: Conceptualization; Methodology; Software; Validation; Formal analysis; Writing – Original Draft; Investigation; Writing – Review & Editing; Visualization. David Barrell: Conceptualization; Methodology; Validation; Writing – Original Draft; Investigation; Writing – Review & Editing; Visualization. Joerg Schaefer: Conceptualization; Methodology; Validation; Investigation; Writing – Review & Editing. Michael Kaplan: Conceptualization; Methodology; Validation; Investigation; Writing – Review & Editing; Funding Acquisition. Peter Strand: Formal analysis; Writing – Review & Editing; Visualization.

Declaration of competing interest

The authors declare that they have no known competing financial interests or personal relationships that could have appeared to influence the work reported in this paper.

Acknowledgements

Funding provided by the Comer Family Foundation, the Quesada Family Foundation, the National Science Foundation, and from the New Zealand Government through the GNS Science 'Global Change through Time' research program (David Barrell). George Denton received support from National Science Foundation grant EAR-1102782. Aaron Putnam and Peter Strand acknowledge support from a National Science Foundation CAREER grant (EAR-1554990). Michael Kaplan acknowledges support from National Science Foundation grant EAR-0745781. Roseanne Schwartz and Jeremy Frisch assisted with laboratory work. Alice Doughty, Samuel Kelley, Kathryn Ladig, and Bess Koffman assisted in the field. We thank the New Zealand Department of Conservation and the individual landowners for permission to carry out the fieldwork. Thanks to Robert F. Anderson who suggested the term Mercer's Paradox and kindly allowed us to make use of it. Peter Huybers kindly provided guidance on constructing the 65°S seasonal duration curve. We thank Helen Bostock for providing us with a vector-based version of the SST diagram (Bostock et al., 2015) used in Fig. 6. Finally, we thank Andrew Lorrey and an anonymous reviewer for thoughtful comments that enabled us to improve the clarity and presentation of the manuscript. This is LDEO contribution no. 8461.

Appendix

Appendix 1. Considerations for surface-exposure dating in the Southern Alps of New Zealand

A1.1. Suitability of greywacke boulders for dating

The predominant bedrock of the eastern Southern Alps consists of quartzofeldspathic sandstone (greywacke) and mudstone (argillite). Hard greywacke boulders transported and deposited by glaciers are well suited for ^{10}Be surface-exposure dating. To what degree are boulders of highly indurated lithic sandstone (i.e., 'greywacke') susceptible to surface erosion, and does this affect the reliability of ^{10}Be age calculations? No erosion corrections have been made in any of the work reported (and the predecessor studies). Although some other researchers do apply erosion corrections, we have not favored this approach for the following reasons.

First, without any robust data on long-term (multi-millennial), meso-scale (square-meter areas) erosion rates in New Zealand greywacke rock, there is no adequate basis for defining a suitable erosion rate for erratic greywacke boulders at our study sites. Second, considerable variability in detail within the parent greywacke rock mass, with meso-scale contrasts in grain-size, cementation and induration, makes it unlikely that there exists a typical rate of rock surface erosion that could be applied in a broad-brush manner to all boulders measured. Third, the protocol we apply for selecting boulders for sampling provides several safeguards, including the avoidance of boulders showing any signs of surface erosion, especially flaking or exfoliation, and the preference for selecting large, flat-topped boulders, on which the products of any slab exfoliation would still likely be sitting. Finally, the general consistency of the results obtained in the work reported here, with good clustering of ages for individual moraine ridges or belts, across

a large number of samples, suggests that erosion sufficient to significantly affect age determinations is not common. If the greywacke lithologies of our selected boulders had been affected by significant erosion, then it would be reasonable to expect more scatter in the data than has been shown to be the case, given the magnitude of erosion can be boulder specific.

A1.2. Suitability of production rate for age calculations

We employed the local 'PNZ2' ^{10}Be production rate determined from the Macaulay valley calibration site (Putnam et al., 2010b), located ~75 km to the northeast of the Lake Pukaki outlet, to calculate all ages reported in this study. This rate has been shown to produce ^{10}Be ages for the ~18-kyr Boundary Stream tarn moraines of the Pukaki right-lateral belt that are in close agreement with ^{14}C age constraints on those moraines (Putnam et al., 2010b). We chose to use the 'Lm' scaling scheme, which includes the Lal (1991)/Stone (2000) scaling model together with the high-resolution geomagnetic model of Lifton et al. (2008), because it produced the best agreement between the Boundary Stream tarn moraines ^{10}Be dates and local ^{14}C control (Putnam et al., 2010b).

A1.3. Updated calculation methods and slight changes to previously published ages

Beryllium-10 concentrations and age calculations reported in Tables S1 and S2 (Supplementary data) utilize updated methods that differ slightly from the methods reported in some previous publications [e.g., (Schaefer et al., 2006, 2009; Kaplan et al., 2010; Putnam et al., 2010a; Kelley et al., 2014)]. These updated methods include the following:

1) We use an updated means of correcting ^{10}Be concentrations for procedural blank backgrounds. This correction involves subtracting the number of ^{10}Be atoms measured in a procedural blank from the total numbers of atoms measured in corresponding samples, rather than subtracting measured blank ^{10}Be/^{9}Be ratios from sample ^{10}Be/^{9}Be ratios.
2) We reference each exposure age to the year A.D. 1950 (to facilitate comparison to ^{14}C chronologies) by subtracting the number of years elapsed between A.D. 1950 and the year in which any given sample was collected.
3) We present 'external' landform age uncertainties (following Putnam et al. (2010a)). These uncertainties were calculated by propagating the standard error of the mean ('SEM') of each distribution, outliers excluded, with a production-rate uncertainty of 2.1%.
4) We fixed typographical errors in some topographic shielding values reported in Kelley et al. (2014).

These methodological updates and fixes result in minor differences between the ages reported in this paper and those reported in the original publications that predate the implementation of these currently used protocols. Relative probability plots of the glacial landform belts of the Pukaki valley are presented in Fig. A1.

Appendix 2. Glacier geometry and relationships with climate

A2.1. Relative glacier lengths and gradients in the Pukaki catchment

Relative to Mt. Tasman, which approximates the mid-point position of the Pukaki catchment head along the Main Divide of the Southern Alps, the mid-to late Holocene glacier termini in the Pukaki catchment (Mueller and Tasman glaciers) lay ~17 km down-valley, the late-glacial 'Birch Hill' terminus of the Pukaki glacier lay ~35 km down-valley, and the 'full-glacial' Tekapo and Mt. John termini of the Pukaki glacier were between ~70 and ~73 km-downvalley (Fig. 4b). We adopt a position of ~75 km down-valley of Mt. Tasman for the 'Balmoral' terminus of the Pukaki glacier. The Birch Hill terminus is approximately 34% of the way from the Holocene termini to the Tekapo terminal position. An ice-molded hill adjacent to the Birch Hill terminal zone yielded an age of 17.5 ± 0.4 kyrs, while the Tekapo moraine belt is 18.1 ± 0.3 kyrs old (see text). Comparing maximum/minimum and minimum/maximum age bounds of the Tekapo moraine belt and of the ice-molded hill indicates that the Pukaki glacier retreated at least two-thirds of the way back to the Holocene ice position in no more than 1.3 kyrs, and no less than 0.1 kyrs.

Relevant topographic features and ice profiles inferred from preserved lateral moraines are plotted the in Fig. 4B profile. The delineation of the 'Birch Hill' and 'Balmoral' terminal positions are discussed below.

There are no preserved Birch Hill terminal moraines, but limits can be placed on its position by consideration of the post-glacial level of Lake Pukaki (Barrell and Read, 2014). If the gradient of the Birch Hill lateral moraine is projected down-valley, it intersects the post-glacial highstand level of Lake Pukaki ~1 km down-valley of the last preserved remnant of lateral moraine. The lateral moraine profile intersects the 'natural modern' level of Lake Pukaki (prior to human intervention for hydro-electric storage (Barrell and Read, 2014)) within ~2 km of the last preserved Birch Hill lateral moraine remnant. It is not known how long the highstand level of the lake persisted, but it is certain that during post-glacial time, the lake was never lower than its 'natural modern' level. These considerations demonstrate that the Birch Hill glacier terminus was no more than 2 km down-valley of the farthest down-valley lateral moraine remnants. The farthest down-valley Birch Hill lateral moraine is ~33.5 km from Mt. Tasman, and hence our adopted value for the terminal position of ~35 km is reasonably conservative.

The down-valley distance of ~75 km for the Balmoral terminus is to the projected distal edge of the terminal moraines of the main ice lobe in the Pukaki valley. However, at this location, there is no preserved Balmoral outwash surface, the moraine belt here has been partially overtopped by Mt. John outwash, and likewise any Balmoral outwash plain that formerly existed in this area. In the left lateral sector of the Pukaki glacier trough was the Maryburn distributary ice lobe. The Maryburn ice lobe extended as much as ~7 km from the main valley at the time the Balmoral moraines were formed (Barrell, 2014; Schaefer et al., 2015). This ice lobe was no more than ~2 km long at early Mt. John time (~37 ka), and did not exist at the time the ~20 kyr Mt. John moraine was formed. And yet it is the ~20 kyr moraine that encroaches farthest over the Balmoral moraines in the Pukaki terminal zone. We think that the most likely explanation is that during the course of the Last Glaciation, the profile of the Pukaki glacier became progressively gentler (see Fig. 4B profile). At Balmoral time, the relatively steep glacier easily overtopped the saddle at the northern end of Mary Range, forming a substantial Maryburn lobe of ice. Progressively through Mt. John time, the glacier became less able, and finally unable, to overtop the topographic divide. The gradient change is also illustrated by the successive overtopping or cutting out of the older components of the Mt. John moraine complex. We think the most likely reason for the progressive gradient change is that the glacial trough was progressively deepened by erosion as the glaciation proceeded (e.g., McKinnon et al., 2012).

A2.2. Climatic interpretation of Pukaki moraines

The changing gradient of the Pukaki glacier over time during the Last Glaciation underscores a need for caution in interpreting the detail of relatively very small variations in glacier extent between moraine belts (Fig. 3) in relation to climate. At face value, modeling the Pukaki glacier in regard to the Balmoral terminal moraines implies a temperature ~7 °C cooler than late 20th century

('modern') temperatures, versus a value of ~ -6.5 °C cooler than modern estimated for the ~20 kyr Mt. John terminal moraine (Schaefer et al., 2015). There is considerable confidence in interpreting the geometry of the glacier trough ~20 kyr ago, because shortly thereafter (~18 kyrs ago), the glacier retreated, leaving a deep trough that was progressively filled with post-glacial sediment. There is no evidence as to the nature of the land surface over which the glacier advanced at Balmoral time. It is tempting to speculate that because this advance followed a prolonged episode of interglacial climate conditions during MIS 5, the trough was deeply filled with interglacial sediments, and probably any post-MIS 6 lake that may have existed had been displaced by sediment. In that case, today's landscape may be a reasonably close analog for the pre-MIS 4 landscape, and modeling the glacier for Balmoral time over the modern topography is probably a satisfactory first approximation.

We follow Kelley et al. (2014) as regarding an episode where the Pukaki glacier occupied its trough sufficiently to leave a preserved lateral moraine as approximating 'full-glacial' conditions, and we infer that each such episode had climatic conditions indistinguishable from any other similar episode.

A2.3. Comment on the grouping of moraine belts

Kelley et al. (2014) noted the presence of four relatively young ages (~36–38 kyr) in the ~42 ka Mt. John moraine belt, and discussed the possibility that they may relate to a younger ice advance. They treated them as statistical outliers in the calculation of the moraine belt age. The identification by Doughty et al. (2015) of moraine ridges of mean age of ~35.5 ka (n = 3) indicates the presence of a moraine belt of that approximate age in the Pukaki moraine sequence. We have therefore combined those three ages with the four ages discussed above from Kelley et al. (2014), to define the ~37 ka moraine belt (Table S2).

In addition, Putnam et al. (2010a) divided the Birch Hill moraine system into two separate belts: Birch Hill I, corresponding to the prominent moraine ridge that defines the outer edge of the belt, and Birch Hill II, which represents the main body of moraine ridges inboard of the Birch Hill I belt. To maintain consistency with our grouping of the Tekapo and Mt. John moraine belts, we chose instead to combine here the Birch Hill I and II belts in our determination of an overall arithmetic mean age, and refer to the full belt of Birch Hill moraine ridges (inboard of the older ~14-kyr outboard moraine knob) as the 'Birch Hill' belt.

A2.4. Estimation of temperatures from glacier records

Glaciological modeling and snowline reconstructions using the accumulation-to-ablation area (AAR) method, both constrained by the mapped and dated glacial landform record, were applied to estimate atmospheric paleotemperatures for the Southern Alps. The results are given in Table S3 and were used to construct the glacier-derived temperature record shown in Fig. 5. The temperature estimates together with the arithmetic mean ^{10}Be age of the constraining landform target provide a glacier-inferred temperature chronology (Fig. 5). Glaciological-modeling–derived temperatures for the Last Glaciation and subsequent deglaciation in the Ohau valley (Kaplan et al., 2010; Doughty et al., 2013; Putnam et al., 2013b) and the Rakaia valley (Putnam et al., 2013a) are supplemented by modeling results for the Pukaki valley (Golledge et al., 2012; Schaefer et al., 2015) and its Whale Stream tributary (Kaplan et al., 2013). Temperature estimates were derived from late-glacial and Holocene moraines in the Pukaki, Ohau, and Cameron catchments using the AAR method (Putnam et al., 2012; Kaplan et al., 2013) and, in the first two localities, were also obtained from glaciological modeling (Putnam et al., 2012; Doughty et al., 2013). The temperature estimate for the Birch Hill moraine belt in the Pukaki valley is also applied to the ~17.5 kyr ice-molded bedrock hill outboard of the Birch Hill moraine belt. Our modeled reconstructions of the Ohau and Pukaki glaciers are generally consistent with those generated by Golledge et al. (2012) using a different glaciological modeling framework. AAR-derived temperatures agree well with those obtained from glaciological modeling (Kaplan et al., 2010, 2013; Doughty et al., 2013), demonstrating convergence among results from different techniques.

Glaciological models referenced temperatures to late 20th century climatological datasets (Birkel et al., 2012; Doughty et al., 2013; Rowan et al., 2013), while AAR reconstructions utilized estimated late 20th century mean snowlines as a baseline for determining snowline depressions, which were converted to temperature values via lapse rates (Kaplan et al., 2010, 2013; Putnam et al., 2012).

For the Last Glaciation and subsequent deglaciation, numerical glaciological models (Birkel et al., 2012; Putnam et al., 2013a, 2013b; Rowan et al., 2013) were forced by temperature lowering until the modeled ice configuration matched the geometry of the mapped landform targets.

Paleotemperature estimates for the Chilean glacial record were derived from correlation to palynological proxy evidence of ecotone altitudes (Denton et al., 1999a, 1999b). The Last Glaciation temperature depression is consistent with that used to model the former Patagonian Ice Sheet configuration to the geometry of the mapped landform targets (Hulton et al., 2002; Hubbard et al., 2005).

Supplementary data

Supplementary data, comprising Tables S1-S3 and a high-resolution version of Fig. 3, to this article can be found online at https://doi.org/10.1016/j.quascirev.2020.106771.

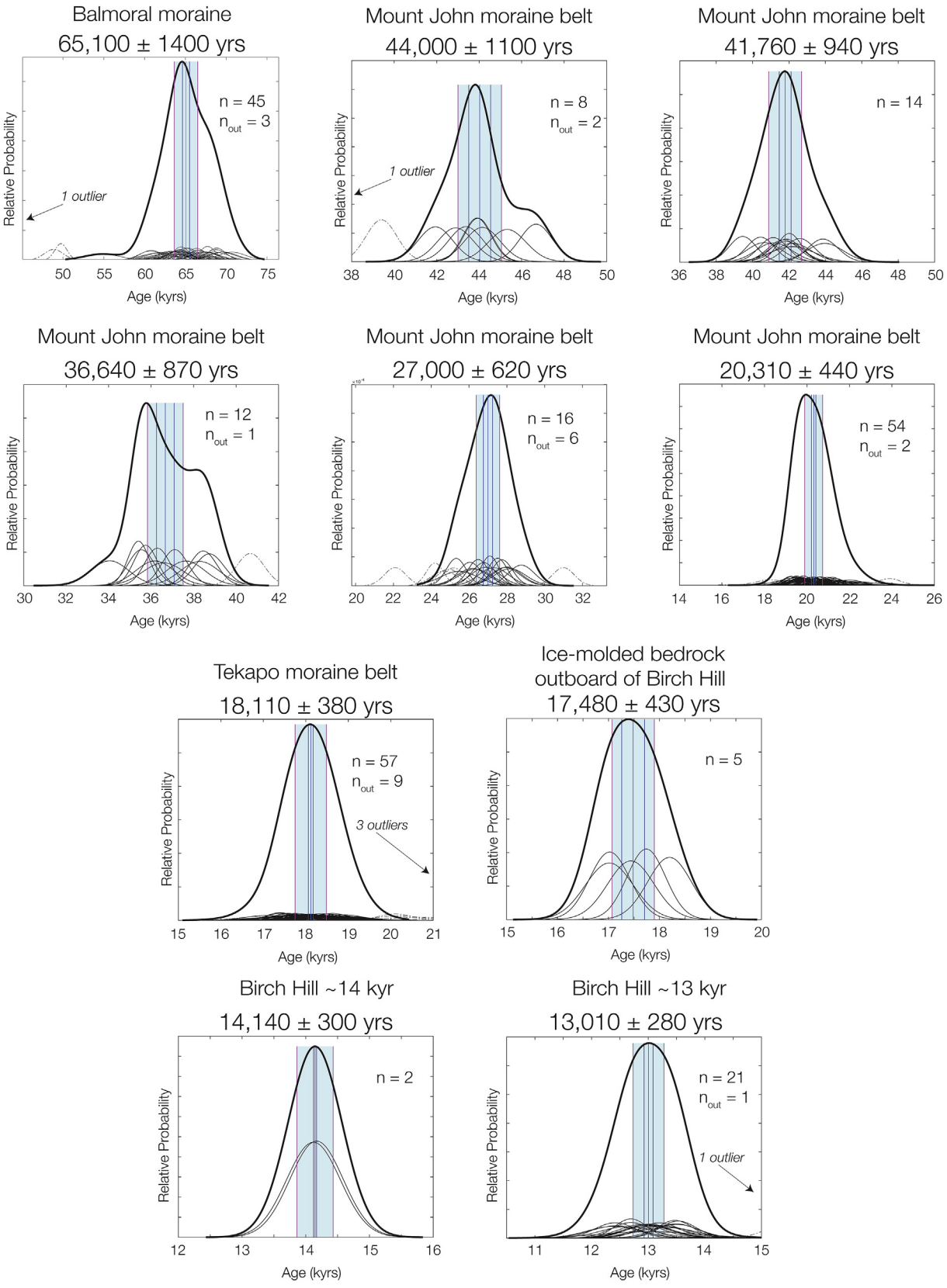

Fig. A1. Relative probability plots for the ten moraine belts dated near Lake Pukaki. Center lines are arithmetic means of reduced data sets, while vertical blue and purple lines are the standard error of the mean and external uncertainty envelopes, respectively. Thin black curves are Gaussian representations of individual ^{10}Be measurements. Thick solid black lines are summed probability curves with outliers pruned. Statistics are summarized in Table S3. Moraine ages are given as the arithmetic mean and external errors (shaded in blue; standard error propagated with production-rate uncertainty).

References

Ahn, J., Brook, E.J., 2008. Atmospheric CO_2 and climate on millennial time scales during the last glacial period. Science 322, 83–85.

Allen, K.A., Sikes, E.L., Hönisch, B., Elmore, A.C., Guilderson, T.P., Rosenthal, Y., Anderson, R.F., 2015. Southwest Pacific deep water carbonate chemistry linked to high southern latitude climate and atmospheric CO_2 during the Last Glacial Termination. Quat. Sci. Rev. 122, 180–191.

Allen, K.A., Sikes, E.L., Anderson, R.F., Rosenthal, Y., 2020. Rapid loss of CO_2 from the South Pacific Ocean during the last glacial termination. Paleoceanography and Paleoclimatology 35, 2019PA003766. https://doi.org/10.1029/2019PA003766.

Andersen, B.G., Denton, G.H., Lowell, T.V., 1999. Glacial geomorphologic maps of Llanquihue drift in the area of the Southern Lake District, Chile. Geogr. Ann. 81, 155–166.

Anderson, B., 2005. Interactive comment on "Synoptic climate change as a driver of late Quaternary glaciations in the mid-latitudes of the Southern Hemisphere" by H. Rother and J. Shulmeister. Clim. Past Discuss 1, S161–S167.

Anderson, B., Lawson, W., Owens, I., Goodsell, B., 2006. Past and future mass balance of 'Ka Roimata o Hine Hukatere' Franz Josef Glacier, New Zealand. J. Glaciol. 52, 597–607.

Anderson, B., Mackintosh, A., 2006. Temperature change is the major driver of late-glacial and Holocene glacier fluctuations in New Zealand. Geology 34, 121–124.

Anderson, B., Mackintosh, A., 2012. Controls on mass balance sensitivity of maritime glaciers in the Southern Alps, New Zealand: The role of debris cover. J. Geophys. Res. 117, F01003.

Anderson, B., Mackintosh, A., Stumm, D., George, L., Kerr, T., Winter-Billington, A., Fitzsimons, S., 2010. Climate sensitivity of a high-precipitation glacier in New Zealand. J. Glaciol. 56, 114–128.

Anderson, R.F., Ali, S., Bradtmiller, L.I., Nielsen, S.H.H., Fleisher, M.Q., Anderson, B.E., Burckle, L.H., 2009. Wind-driven upwelling in the Southern Ocean and the deglacial rise in atmospheric CO_2. Science 323, 1443–1448.

Ayliffe, L.K., Gagan, M.K., Zhao, J.-x., Drysdale, R.N., Hellstrom, J.C., Hantoro, W.S., Griffiths, M.L., Scott-Gagan, H., St Pierre, E., Cowley, J.A., Suwargadi, B.W., 2013. Australasian monsoon sensitivity to millennial climate change during the last deglaciation. Nat. Commun. https://doi.org/10.10138/ncomms13908.

Bard, E., Rickaby, R.E.M., 2009. Migration of the subtropical front as a modulator of glacial climate. Nature 460, 380–383.

Bard, E., Rostek, F., Turon, J.L., Gendreau, S., 2000. Hydrological impact of Heinrich events in the subtropical northeast Atlantic. Science 289, 1321–1324.

Barker, S., Diz, P., Vautravers, M.J., Pike, J., Knorr, G., Hall, I.R., Broecker, W.S., 2009. Interhemispheric Atlantic seesaw response during the last deglaciation. Nature 457, 1097–1102.

Barker, S., Chen, J., Gong, X., Jonkers, L., Knorr, G., Thornalley, D., 2015. Icebergs not the trigger for North Atlantic cold events. Nature 520, 333–336.

Barrell, D.J.A., 2011. Quaternary glaciers of New Zealand. In: Ehlers, J., Gibbard, P.L., Hughes, P.D. (Eds.), Quaternary Glaciations, Extent and Chronology: A Closer Look, vol. 15. Elsevier. Developments in Quaternary Science, Amsterdam, pp. 1047–1064.

Barrell, D.J.A., 2014. The Balmoral moraines near Lake Pukaki, Southern Alps: A new reference area for the early Otira Glaciation in New Zealand. N. Z. J. Geol. Geophys. 57, 442–452.

Barrell, D.J.A., Almond, P.C., Vandergoes, M.J., Lowe, D.J., Newnham, R.M., 2013. A composite pollen-based stratotype for inter-regional evaluation of climatic events in New Zealand over the past 30,000 years (NZ-INTIMATE project). Quat. Sci. Rev. 74, 4–20.

Barrell, D.J.A., Andersen, B.G., Denton, G.H., 2011. Glacial geomorphology of the central South Island, New Zealand. GNS Science Monograph 27.

Barrell, D.J.A., Putnam, A.E., Denton, G.H., 2019a. Reconciling the onset of deglaciation in the upper Rangitata valley, Southern Alps, New Zealand. Quat. Sci. Rev. 203, 141–150.

Barrell, D.J.A., Putnam, A.E., Denton, G.H., 2019b. Reply to comment received from J. Shulmeister et al. regarding "Reconciling the onset of deglaciation in the upper Rangitata valley, Southern Alps, New Zealand". Quat. Sci. Rev. 219, 316–318.

Barrell, D.J.A., Read, S.A.L., 2014. The deglaciation of Lake Pukaki, South Island, New Zealand—a review. N. Z. J. Geol. Geophys. 57, 86–101.

Barrows, T.T., Juggins, S., De Deckker, P., Calvo, E., Pelejero, C., 2007. Long-term sea surface temperature and climate change in the Australian-New Zealand region. Paleoceanography 22, PA22215.

Bendle, J.M., Palmer, A.P., Thorndycroft, V.R., Matthews, I.P., 2019. Phased Patagonian Ice Sheet response to Southern Hemisphere atmospheric and oceanic warming between 18 and 17 ka. Sci. Rep. 9, 4133.

Biastoch, A., Böning, C.W., Schwarzkopf, F.U, 2009. Lutjeharms, J.R.E. Increase in Agulhas leakage due to poleward shift of Southern Hemisphere westerlies. Nature 462, 495–498.

Birkel, S.D., Putnam, A.E., Denton, G.H., Koons, P.O., Fastook, J.L., Putnam, D.E., Maasch, K.A., 2012. Climate inferences from a glaciological reconstruction of the Late Pleistocene Wind River Ice Cap, Wind River Range, Wyoming. Arctic Antarct. Alpine Res. 44, 265–276.

Boex, J., Fogwill, C., Harrison, S., Glasser, N.F., Hein, A., Schnabel, C., Xu, S., 2013. Rapid thinning of the late Pleistocene Patagonian Ice Sheet followed migration of the southern westerlies. Sci. Rep. 3, 2118.

Bond, G., Heinrich, H., Broecker, W., Labeyrie, L., McManus, J., Andrews, J., Huon, S., Jantschik, R., Clasen, S., Simet, C., Tedesco, K., Klas, M., Bonani, G., Ivy, S., 1992. Evidence for massive discharges of icebergs into the North Atlantic ocean during the last glacial period. Nature 360, 245–249.

Bond, G.C., Lotti, R., 1995. Iceberg discharges into the North Atlantic on millennial time scales during the Last Glaciation. Science 267, 1005–1010.

Bostock, H.C., Barrows, T.T., Carter, L., Chase, Z., Cortese, G., Dunbar, G.B., Ellwood, M., Hayward, B., Howard, W., Neil, H.L., Noble, T.L., Mackintosh, A., Moss, P.T., Moy, A.D., White, D., Williams, M.J.M., Armand, L.K., 2013. A review of the Australian-New Zealand sector of the Southern Ocean over the last 30 ka (Aus-INTIMATE project). Quat. Sci. Rev. 74, 35–57.

Bostock, H.C., Hayward, B.W., Neil, H.L., Sabaa, A.T., Scott, G.H., 2015. Changes in the position of the Subtropical Front south of New Zealand since the last glacial period. Paleoceanography 30, 824–844.

Bostock, H.C., Opdyke, B.N., Gagan, M.K., Kiss, A.E., Fifield, L.K., 2006. Glacial/interglacial changes in the East Australian current. Clim. Dynam. 26, 645–659.

Boswell, S.M., Toucanne, S., Pitel-Roudaut, M., Creyts, T.T., Eynaud, F., Bayon, G., 2019. Enhanced surface melting of the Fennoscandian Ice Sheet during periods of North Atlantic cooling. Geology 47, 664–668. https://doi.org/10.1130/G46370.1.

Bracegirdle, T.J., Shuckburgh, E., Sallee, J.-B., Wang, Z., Meijers, A.J.S., Bruneau, N., Phillips, T., Wilcox, L.J., 2013. Assessment of surface winds over the Atlantic, Indian, and Pacific Ocean sectors of the Southern Ocean in CMIP5 models: Historical bias, forcing response, and state dependence. J. Geophys. Res.: Atmosphere 118, 547–562.

Broccoli, A.J., Dahl, K.A., Stouffer, R.J., 2006. Response of the ITCZ to Northern Hemisphere cooling. Geophys. Res. Lett. 33, L01702.

Broecker, W.S., 1978. The cause of glacial to interglacial climatic change. In: Gautier, D. (Ed.), Evolution of Planetary Atmospheres and Climatology of the Earth: Toulouse, France. Centre National d'Etudes Spatiales, pp. 165–190.

Broecker, W.S., Bond, G., Klas, M., Clark, E., McManus, J., 1992. Origin of the northern Atlantic's Heinrich events. Clim. Dynam. 6, 265–273.

Broecker, W.S., Denton, G.H., 1989. The role of ocean-atmosphere reorganizations in glacial cycles. Geochem. Cosmochim. Acta 53, 2465–2501.

Broecker, W.S., Putnam, A.E., 2012. How did the hydrologic cycle respond to the two-phase mystery interval? Quat. Sci. Rev. 57, 17–25.

Broecker, W.S., Putnam, A.E., 2013. Hydrologic impacts of past shifts of Earth's thermal equator offer insight into those to be produced by fossil fuel CO_2. Proc. Natl. Acad. Sci. Unit. States Am. 110, 16710–16715.

Bronselaer, B., Winton, M., Griffies, S.M., Hurlin, W.J., Rodgers, K.B., Sergienko, O.V., Stouffer, R.J., Russell, J.L., 2018. Change in future climate due to Antarctic meltwater. Nature 564, 53–58.

Bronselaer, B., Winton, M., Russell, J., Sabine, C.L., Khatiwala, S., 2017. Agreement of CMIP5 simulated and observed ocean anthropogenic CO_2 uptake. Geophys. Res. Lett. 44, 12,298–12,305.

Brook, E.J., Buizert, C., 2018. Antarctic and global climate history viewed from ice cores. Nature 558, 200–208.

Buizert, C., Cuffey, K.M., Severinghaus, J.P., Baggenstos, D., Fudge, T.J., Steig, E.J., Markle, B.R., Winstrup, M., Rhodes, R.H., Brook, E.J., Sowers, T.A., Clow, G.D., Cheng, H., Edwards, R.L., Sigl, M., McConnell, J.R., Taylor, K.C., 2015. The WAIS Divide deep ice core WD2014 chronology — Part 1: Methane synchronization (68-31 ka BP) and the gas age-ice age difference. Clim. Past 11, 153–173.

Buizert, C., Gkinis, V., Severinghaus, J.P., He, F., Lacavalier, B.S., Kindler, P., Leuenberger, M., Carlson, A.E., Vinther, B., Masson-Delmotte, V., White, J.W.C., Liu, Z., Otto-Bliesner, B., Brook, E.J., 2014. Greenland temperature response to climate forcing during the last deglaciation. Science 345, 1177–1180.

Burga, C.A., 1988. Swiss vegetation history during the last 18,000 years. New Phytol. 110, 581–602.

Burke, A., Robinson, L.F., 2012. The Southern Ocean's role in carbon exchange during the last deglaciation. Science 335, 558–561.

Cai, W., Shi, G., Cowan, T., Bi, D., Ribbe, J., 2005. The response of the Southern Annular Mode, the East Australian Current, and the southern mid-latitude ocean circulation to global warming. Geophys. Res. Lett. 32 (23), 2005GL024701 https://doi.org/10.1029/2005GL024701.

Cane, M.A., 1998. A role for the tropical Pacific. Science 282, 59–61.

Cheng, H., Edwards, R.L., Broecker, W.S., Denton, G.H., Kong, K., Wanf, Y., Zang, R., Wang, Z., 2009. Ice age terminations. Science 326, 248–252.

Chinn, T.J.H., 2012. Annual ice volume changes 1976-2008 for the New Zealand Southern Alps. Global Planet. Change 92, 105–118.

Clark, C.D., Hughes, A.L.C., Greenwood, S.L., Jordan, C., Sejrup, H.P., 2012. Pattern and timing of retreat of the last British-Irish Ice Sheet. Quat. Sci. Rev. 44, 112–146. https://doi.org/10.1016/j.quascirev.2010.07.019.

Clark, P.U., Dyke, A.S., Shakun, J.D., Carlson, A.E., Clark, J., Wohlfarth, B., Mitrovica, J.X., Hostetler, S.W., McCabe, A.M., 2009. The last glacial maximum. Science 325, 710–714.

Colhoun, E.A., Barrows, T.T., 2011. The glaciation of Australia. In: Ehlers, J., Gibbard, P.L., Hughes, P.D. (Eds.), Quaternary Glaciations, Extent and Chronology: A Closer Look, vol. 15. Elsevier. Developments in Quaternary Science, Amsterdam, pp. 1037–1045.

Cuffey, K.M., Clow, G.D., Steig, E.J., Buizert, C., Fudge, T.J., Koutnik, M., Waddington, E.D., Alley, R.B., Severinghaus, J.P., 2016. Deglacial temperature history of West Antarctica. Proc. Natl. Acad. Sci. Unit. States Am. 113, 14249–14254.

Dalton, A.S., Margold, M., Stokes, C.R., Tarasov, L., Dyke, A.S., Adams, R.S., Allard, S., Arends, H.E., Atkinson, N., Attig, J.W., et al., 2020. An updated radiocarbon-based ice margin chronology for the last deglaciation of the North American Ice Sheet Complex. Quat. Sci. Rev. 234, 106223 https://doi.org/10.1016/j.quascirev.2020.106223.

Darvill, C.M., Bentley, M.J., Stokes, C.R., Shulmeister, J., 2016. The timing and cause of glacial advances in the southern mid-latitudes during the last glacial cycle based on a synthesis of exposure ages from Patagonia and New Zealand. Quat. Sci. Rev. 149, 200–214.

Davies, B.J., Darvill, C.M., Lovell, H., Bendle, J.M., Dowdeswell, J.A., Fabel, D., García, J.-L., Geiger, A., Glasser, N.F., Gheorghiue, D.M., Harrison, S., Kaplan, M.R., Martina, J.R.V., Mendelovai, M., Palmer, A., Peltok, M., Rodése, A., Sagredo, E.A., Smedley, R.K., Smellie, J.L., Thorndycraft, V.R., 2020. The evolution of the Patagonian Ice Sheet from 35 ka to the present day (PATICE). Earth Sci. Rev. 204, 103152.

De Deckker, P., Moros, M., Perner, K., Jansen, E., 2012. Influence of the tropics and southern westerlies on glacial interhemispheric asymmetry. Nat. Geosci. 5, 266–269.

Delworth, T.L., Zeng, F.R., 2008. Simulated impact of altered Southern Hemisphere winds on the Atlantic Meridional Overturning Circulation. Geophys. Res. Lett. 35, L20708.

Denton, G.H., Broecker, W.S., Alley, R.B., 2006. The mystery interval 17.5 to 14.5 kyrs ago. PAGES News 14, 14–16.

Denton, G.H., Alley, R.B., Comer, G.C., Broecker, W.S., 2005. The role of seasonality in abrupt climate change. Quat. Sci. Rev. 24, 1159–1182.

Denton, G.H., Anderson, R.F., Toggweiler, J.R., Edwards, R.L., Schaefer, J.M., Putnam, A.E., 2010. The last glacial termination. Science 328, 1652–1656.

Denton, G.H., Heusser, C.J., Lowell, T.V., Moreno, P.I., Andersen, B.G., Heusser, L.E., Schlüchter, C., Marchant, D.R., 1999a. Interhemispheric linkage of paleoclimate during the last glaciation. Geogr. Ann. 81A, 107–153.

Denton, G.H., Hughes, T.J., 2002. Reconstructing the Antarctic Ice Sheet at the Last Glacial Maximum. Quat. Sci. Rev. 21, 193–202.

Denton, G.H., Lowell, T.V., Heusser, C.J., Schlüchter, C., Andersen, B.G., Heusser, L.E., Moreno, P.I., Marchant, D.R., 1999b. Geomorphology, stratigraphy, and radiocarbon chronology of Llanquihue drift in the area of the Southern Lake District, Seno Reloncaví, and Isla Grande de Chiloé, Chile. Geogr. Ann. 81A, 167–229.

Doughty, A.M., Anderson, B.M., Mackintosh, A.N., Kaplan, M.R., Vandergoes, M.J., Barrell, D.J.A., Denton, G.H., Schaefer, J.M., Chinn, T.J.H., Putnam, A.E., 2013. Evaluation of Lateglacial temperatures in the Southern Alps of New Zealand based on glacier modelling at Irishman Stream, Ben Ohau Range. Quat. Sci. Rev. 74, 160–169.

Doughty, A.M., Schaefer, J.M., Denton, G.H., Kaplan, M.R., Putnam, A.E., Andersen, B.G., Barrell, D.J.A., Schwartz, R., Finkel, R.C., 2015. Mismatch of glacier extent and summer insolation in Southern Hemisphere mid-latitudes. Geology 43, 407–410. https://doi.org/10.1130/G36477.36471.

Dowey, C.W., 2015. Glacier fluctuations during Termination 1 in Mackenzie Stream valley, Southern Alps, New Zealand. MSc Thesis (Earth and Climate Sciences). University of Maine, USA.

Dunne, J.P., John, J.G., Adcroft, A.J., Griffies, S.M., Hallberg, R.W., Shevliakova, E., Stouffer, R.J., Cooke, W., Dunne, K.A., Harrison, M.J., Krasting, J.P., Malyshev, S.L., Milly, P.C.D., Phillipps, P.J., Sentman, L.T., Samuels, B.L., Spelman, M.J., Winton, M., Wittenberg, A.T., Zadeh, N., 2012. GFDL's ESM2 global coupled climate–carbon Earth System Models. Part I: Physical formulation and baseline simulation characteristics. J. Clim. 25, 6646–6665.

Dunne, J.P., John, J.G., Shevliakova, E., Stouffer, R.J., Krasting, J.P., Malyshev, S.L., Milly, P.C.D., Sentman, L.T., Adcroft, A.J., Cooke, W., Dunne, K.A., Griffies, S.M., Hallberg, R.W., Harrison, M.J., Levy, H., Wittenberg, A.T., Phillips, P.J., Zadeh, N., 2013. GFDL's ESM2 global coupled climate–carbon Earth System Models. Part II: Carbon system formulation and baseline simulation characteristics. J. Clim. 26, 2247–2267.

Dykoski, C.A., Edwards, R.L., Cheng, H., Yuan, D., Cai, Y., Zhang, M., Lin, Y., Qing, J., An, Z., Revenaugh, J., 2005. A high-resolution, absolute-dated Holocene and deglacial Asian monsoon record from Dongee Cave, China. Earth Planet Sci. Lett. 233, 71–86.

Eaves, S.R., Anderson, B.M., Mackintosh, A.N., 2017. Glacier-based climate reconstructions for the last glacial–interglacial transition: Arthur's Pass, New Zealand (43°S). J. Quat. Sci. 32, 877–887.

Eaves, S.R., Brook, M.S., 2021. Glaciers and glaciation of North Island, New Zealand. N. Z. J. Geol. Geophys. 64, 1–20. https://doi.org/10.1080/00288306.2020.1811354 (in press).

Fasullo, J.T., Trenberth, K.E., 2008. The annual cycle of the energy budget. Part II: Meridional structures and poleward transports. J. Clim. 21, 2313–2325.

Florineth, D., Schlüchter, C., 1998. Reconstructing the Last Glacial Maximum (LGM) ice surface geometry and flowlines in the Central Swiss Alps. Eclogae Geol. Helv. 91, 391–407.

Florineth, D., Schlüchter, C., 2000. Alpine evidence for atmospheric circulation patterns in Europe during the last glacial maximum. Quat. Res. 54, 295–308.

Fogwill, C.J., Turney, C.S.M., Hutchinson, D.K., Taschetto, A.S., England, M.H., 2015. Obliquity control on Southern Hemisphere climate during the last glacial. Sci. Rep. 5, 11673.

Fogwill, C.J., Turney, C.S.M., Menviel, L., et al., 2020. Southern Ocean carbon sink enhanced by sea-ice feedbacks at the Antarctic Cold Reversal. Nat. Geosci. 13, 489–497. https://doi.org/10.1038/s41561-020-0587-0.

García, J.-L., Hein, A.S., Binnie, S.A., Gomez, G.A., Gonzalez, M.A., Dunai, T.J., 2018. The MIS 3 maximum of the Torres del Paine and Última Esperanza ice lobes in Patagonia and the pacing of southern mountain glaciation. Quat. Sci. Rev. 185, 9–26.

Gillett, N.P., Thompson, D.W.J., 2003. Simulation of recent Southern Hemisphere climate change. Science 302, 273–275.

Godfrey, J.S., 1989. A Sverdrup model of the depth-integrated flow for the world ocean allowing for island circulations. Geophys. Astrophys. Fluid Dynam. 45, 89–112.

Golledge, N.R., Mackintosh, A.N., Anderson, B.M., Buckley, K.M., Doughty, A.M., Barrell, D.J.A., Denton, G.H., Vandergoes, M.J., Andersen, B.G., Schaefer, J.M., 2012. Last Glacial Maximum climate in New Zealand inferred from a modelled Southern Alps icefield. Quat. Sci. Rev. 46, 30–45.

Gottschalk, J., Skinner, L., Lippold, J., Vogel, H., Frank, N., Jaccard, S.L., Waelbroeck, C., 2016. Biological and physical controls in the Southern Ocean on past millennial-scale atmospheric CO_2 changes. Nat. Commun. 7, 11539 https://doi.org/10.1038/ncomms11539.

Grimm, E.C., Watts, W.A., Jacobson Jr., G.L., Hansen, B.C.S., Almquist, H.R., Dieffenbacher-Krall, A.C., 2006. Evidence for warm wet Heinrich events in Florida. Quat. Sci. Rev. 25, 2197–2211.

Grousset, F.E., Cortijo, E., Huon, S., Hervé, L., Richter, T., Burdloff, D., Duprat, J., Weber, O., 2001. Zooming in on Heinrich layers. Paleoceanography 16, 240–259.

Hall, B.L., Porter, C.T., Denton, G.H., Lowell, T.V., Bromley, G.R.M., 2013. Extensive recession of Cordillera Darwin glaciers in southernmost South America during Heinrich Stadial 1. Quat. Sci. Rev. 62, 49–55.

Hall, B.L., Denton, G.H., Heath, S.L., Jackson, M.S., Koffman, T.N.B., 2015. Accumulation and marine forcing of ice dynamics in the western Ross Sea during the last deglaciation. Nat. Geosci. 8, 625–628.

Hall, B.L., Lowell, T.V., Bromley, G.R.M., Denton, G.H., Putnam, A.E., 2019. Holocene glacier fluctuations on the northern flank of Cordillera Darwin, southernmost South America. Quat. Sci. Rev. 222, 105904.

Harrington, H.J., 1952. Glacier wasting and retreat in the Southern Alps of New Zealand. J. Glaciol. 2, 140–144.

Haumann, A.F., Gruber, N., Münnich, M., 2020. Sea-ice induced Southern Ocean subsurface warming and surface cooling in a warming climate. AGU Advances 1, e2019AV000132.

Hays, J.D., Imbrie, J., Shackleton, N.J., 1976. Variations in the Earth's orbit: pacemaker of the Ice Ages. Science 194 (4270), 1121–1132.

He, F., Shakun, J.D., Clark, P.U., Carlson, A.E., Liu, Z., Otto-Bliesner, B.L., Kutzbach, J.E., 2013. Northern Hemisphere forcing of Southern Hemisphere climate during the last deglaciation. Nature 494, 81–85.

Heusser, C.J., 1989. Southern westerlies during the Last Glacial Maximum. Quat. Res. 31, 423–425.

Hill, K.L., Rintoul, S.R., Coleman, R., Ridgway, K.R., 2008. Wind forced low frequency variability of the East Australia Current. Geophys. Res. Lett. 35, L08602.

Hodell, D.A., Nicholl, J.A., Bontognali, T.R.R., Danino, S., Dorador, J., Dowdeswell, J.A., Einsle, J., Kuhlmann, H., Martrat, B., Mleneck-Vautravers, M.J., Rodríguez-Tovar, F.J., Röhl, U., 2017. Anatomy of Heinrich Layer 1 and its role in the last deglaciation. Paleoceanography 32, 284–303.

Hubbard, A., Hein, A.S., Kaplan, M.R., Hulton, N.R.J., Glasser, N., 2005. A modelling reconstruction of the last glacial maximum ice sheet and its deglaciation in the vicinity of the Northern Patagonian Icefield, South America. Geogr. Ann. 87A, 375–391.

Hughes, A.L.C., Gyllencreutz, R., Lohne, Ø.S., Mangerud, J., Svendsen, J.I., 2016. The last Eurasian ice sheets – a chronological database and time-slice reconstruction: DATED-1. Boreas 45, 1–45.

Hulton, N.R.J., Purves, R.S., McCulloch, R.D., Sugden, D.E., Bentley, M.J., 2002. The Last Glacial Maximum and deglaciation in southern South America. Quat. Sci. Rev. 21, 233–241.

Huybers, P., 2006. Early Pleistocene glacial cycles and the integrated summer insolation forcing. Science 313, 508–511.

Huybers, P., 2009. Antarctica's orbital beat. Science 325, 1085–1086.

Huybers, P., 2011. Combined obliquity and precession pacing of late Pleistocene deglaciations. Nature 480, 229–232.

Huybers, P., Denton, G., 2008. Antarctic temperature at orbital timescales controlled by local summer duration. Nat. Geosci. 1, 787–792.

Indermühle, A., Monnin, E., Stauffer, B., Stocker, T.F., Wahlen, M., 2000. Atmospheric CO_2 concentration from 60 to 20 kyr BP from the Taylor Dome ice core, Antarctica. Geophys. Res. Lett. 27, 735–738.

Isarin, R.F.B., Renssen, H., 1999. Reconstructing and modelling Late Weichselian climates: the Younger Dryas in Europe as a case study. Earth Sci. Rev. 48, 1–38.

Isarin, R.F.B., Renssen, H., Vandenberghe, J., 1998. The impact of the North Atlantic Ocean on the Younger Dryas climate in northwestern and central Europe. J. Quat. Sci. 13, 447–453.

Ivy-Ochs, S., 2015. Glacier variations in the European Alps at the end of the last glaciation. Cuadernos de Investigacion Geografica 41, 295–315.

Jaccard, S.L., Galbraith, E.D., Martínez-García, A., Anderson, R.F., 2016. Covariation of deep Southern Ocean oxygenation and atmospheric CO_2 through the last ice age. Nature 530 (7589), 207–210. https://doi.org/10.1038/nature16514.

Kaiser, J., Lamy, F., Hebbeln, D., 2005. A 70-kyr sea surface temperature record off southern Chile (Ocean Drilling Program Site 1233). Paleoceanography 20, PA4009.

Kanner, L.C., Burns, S.J., Cheng, H., Edwards, R.L., 2012. High-latitude forcing of the South American summer monsoon during the last glacial. Science 335, 570–573.

Kaplan, M.R., Ackert Jr., R.P., Singer, B.S., Douglass, D.C., Kurz, M.D., 2004. Cosmogenic nuclide chronology of millennial-scale glacial advances during O-isotope stage 2 in Patagonia. Geol. Soc. Am. Bull. 116, 308–321.

Kaplan, M.R., Fogwill, C.J., Sugden, D.E., Hulton, N., Kubik, P.W., Freeman, S., 2008a. Southern Patagonian glacial chronology for the last glacial period and implications for Southern Ocean climate. Quat. Sci. Rev. 27, 284–294.

Kaplan, M.R., Moreno, P.I., Rojas, M., 2008b. Glacial dynamics in southernmost

South America during Marine Isotope Stage 5e to the Younger Dryas chron: A brief review with a focus on cosmogenic nuclide measurements. J. Quat. Sci. 23, 649–658.
Kaplan, M.R., Schaefer, J.M., Denton, G.H., Barrell, D.J.A., Chinn, T.J.H., Putnam, A.E., Andersen, B.G., Finkel, R.C., Schwartz, R., Doughty, A.M., 2010. Glacier retreat in New Zealand during the Younger Dryas stadial. Nature 467, 194–197.
Kaplan, M.R., Schaefer, J.M., Denton, G.H., Doughty, A.M., Barrell, D.J.A., Chinn, T.J.H., Putnam, A.E., Andersen, B.G., Mackintosh, A., Finkel, R.C., Schwartz, R., Anderson, B., 2013. The anatomy of long-term warming since 15 kyr ago in New Zealand based on net glacier snowline rise. Geology 41, 887–890.
Kawamura, K., Parrenin, F., Lisiecki, L., Uemura, R., Vimeux, F., Severinghaus, J.P., Hutterli, M.A., Nakazawa, T., Aoki, S., Jouzel, J., Raymo, M.E., Matsumoto, K., Nakata, H., Motoyama, H., Fujita, S., Goto-Azuma, K., Fujii, Y., Watanabe, O., 2007. Northern Hemisphere forcing of climatic cycles in Antarctica over the past 360,000 years. Nature 448, 912–916.
Kelley, S.E., Kaplan, M.R., Schaefer, J.M., Andersen, B.G., Barrell, D.J.A., Putnam, A.E., Denton, G.H., Schwartz, R., Finkel, R.C., Doughty, A.M., 2014. High-precision ^{10}Be chronology of moraines in the Southern Alps indicates synchronous cooling in Antarctica and New Zealand 42,000 years ago. Earth Planet Sci. Lett. 405, 194–206.
Koester, A.J., Shakun, J.D., Bierman, P.R., Davis, P.T., Corbett, L.B., Braun, D., Zimmerman, S.R., 2017. Rapid thinning of the Laurentide Ice Sheet in coastal Maine, USA, during late Heinrich Stadial 1. Quat. Sci. Rev. 163, 180–192.
Koffman, T.N.B., Schaefer, J.M., Putnam, A.E., Denton, G.H., Barrell, D.J.A., Rowan, A.V., Finkel, R.C., Rood, D.H., Schwartz, R., Plummer, M.A., Brocklehurst, S.H., 2017. A beryllium-10 chronology of late-glacial moraines in the upper Rakaia valley, Southern Alps, New Zealand supports Southern-Hemisphere warming during the Younger Dryas. Quat. Sci. Rev. 170, 14–25.
Kohfeld, K.E., Graham, R.M., de Boer, A.M., Sime, L.C., Wolff, E.W., Le Quéré, C., Bopp, L., 2013. Southern Hemisphere westerly wind changes during the Last Glacial Maximum: Paleo-data synthesis. Quat. Sci. Rev. 68, 76–95.
Lal, D., 1991. Cosmic-ray labeling of erosion surfaces: In situ nuclide production rates and erosion models. Earth Planet Sci. Lett. 104, 424–439.
Lamy, F., Hebbeln, D., Wefer, G., 1998. Late Quaternary precessional cycles of terrigenous sediment input off the Norte Chico, Chile (27.5°S) and palaeoclimatic implications. Palaeogeogr. Palaeoclimatol. Palaeoecol. 141, 233–251.
Lamy, F., Kilian, R., Arz, H., Francois, J.-P., Kaiser, J., Prange, M., Steinke, T., 2010. Holocene changes in the position and intensity of the southern westerly wind belt. Nat. Geosci. 3, 695–699. https://doi.org/10.1038/ngeo959.
Lamy, F., Kaiser, J., Arz, H.W., Hebbeln, D., Ninnemann, U., Timm, O., Timmermann, A., Toggweiler, J.R., 2007. Modulation of the bipolar seesaw in the southeast Pacific during Termination 1. Earth Planet Sci. Lett. 259, 400–413.
Lamy, F., Kaiser, J., Ninnemann, U., Hebbeln, D., Arz, H.W., Stoner, J., 2004. Antarctic timing of surface water changes off Chile and Patagonian ice sheet response. Science 304, 1959–1962.
Lee, S.-Y., Chiang, J.C.H., Matsumoto, K., Tokos, K.S., 2011. Southern Ocean wind response to North Atlantic cooling and the rise in atmospheric CO_2: modeling perspective and paleoceanographic implications. Paleoceanography 26, PA1214. https://doi.org/10.1029/2010PA002004.
Lifton, N., Smart, B., Shea, M., 2008. Scaling time-integrated in situ cosmogenic nuclide production rates using a continuous geomagnetic model. Earth Planet Sci. Lett. 268, 190–201.
Lopes dos Santos, R.A., Spooner, M.I., Barrows, T.T., De Deckker, P., Sinninghe Damsté, J.S., Schouten, S., 2013. Comparison of organic (UK'_{37}, TEX^H_{86}, LDI) and faunal proxies (foraminiferal assemblages) for reconstruction of late Quaternary sea surface temperature variability from offshore southeastern Australia. Paleoceanography 28, 1–11. https://doi.org/10.1002/palo.20035.
Lorrey, A.M., Bostock, H., 2017. The Quaternary climate of New Zealand. Advances in Quaternary Science - the New Zealand Landscape. Springer-Verlag, pp. 67–139.
Lorrey, A.M., Fauchereau, N., Stanton, C., Chappell, P.R., Phipps, S.J., Mackintosh, A., Renwick, J.A., Fowler, A.M., 2014. The Little Ice Age climate of New Zealand reconstructed from Southern Alps cirque glaciers: a synoptic type approach. Clim. Dynam. 42, 3039–3060. https://doi.org/10.1077/s00382-013-1876-8.
Lorrey, A.M., Williams, P.W., Salinger, J., Martin, T.J., Fowler, A.M., Zhao, J.-X., Neil, H., 2008. Speleothem stable isotope records interpreted within a multi-proxy framework and implications for New Zealand palaeoclimate reconstruction. Quat. Int. 187, 52–75.
Lorrey, A.M., Williams, P.W., Woolley, J.-M., Hartland, A., Bostock, H., Eaves, S., Lachniet, M.S., Renwick, J.A., Varma, V., 2020. Late Quaternary climate variability and change from Aotearoa New Zealand speleothems: Progress in age modelling, oxygen isotope master record construction and proxy-model comparisons. Quaternary 3 (3), 24. https://doi.org/10.3390/quat3030024.
Mackintosh, A.N., Anderson, B.M., Pierrehumbert, R.T., 2017. Reconstructing climate from glaciers. Annu. Rev. Earth Planet Sci. 45, 649–680.
Marcott, S.A., Bauska, T.K., Buizert, C., Steig, E.J., Rosen, J.L., Cuffey, K.M., Fudge, T.J., Severinghaus, J.P., Ahn, J., Kalk, M.L., McConnell, J.R., Sowers, T., Taylor, K.C., White, J.W.C., Brook, E.J., 2014. Centennial-scale changes in the global carbon cycle during the last deglaciation. Nature 514, 616–619.
Marcott, S.A., Clark, P.U., Padman, L., Klinkhammer, G.P., Springer, S.R., Liu, Z., Otto-Bleisner, B.L., Carlson, A.E., Ungerer, A., Padman, J., He, F., Cheng, J., Schmittner, A., 2011. Ice-shelf collapse from subsurface warming as a trigger for Heinrich events. Proc. Natl. Acad. Sci. Unit. States Am. 108 (33), 13415–13419.
Margold, M., Stokes, C.R., Clark, C.D., 2018. Reconciling records of ice streaming and ice margin retreat to produce a palaeogeographic reconstruction of the deglaciation of the Laurentide Ice Sheet. Quat. Sci. Rev. 189, 1–30. https://doi.org/10.1016/j.quascirev.2018.03.013.
Markle, B.R., Steig, E.J., Buizert, C., Schoenemann, S.W., Bitz, C.M., Fudge, T.J., Pedro, J.B., Ding, Q., Jones, T.R., White, J.W.C., Sowers, T., 2017. Global atmospheric teleconnections during Dansgaard–Oeschger events. Nat. Geosci. 10, 36–40.
Martin, L.C.P., Blard, P.-H., Lavé, J., Jomelli, V., Charreau, J., Condom, T., Lupker, M., ASTER Team, 2020. Antarctic-like temperature variations in the Tropical Andes recorded by glaciers and lakes during the last deglaciation. Quat. Sci. Rev. 247, 106542.
Mayewski, P.A., Carleton, A.M., Birkel, S.D., Dixon, D., Kurbatov, A.V., Korotkikh, E., McConnell, J., Curran, M., Cole-Dai, J., Jiang, S., Plummer, C., Vance, T., Maasch, K.A., Sneed, S.B., Handley, M., 2017. Ice core and climate reanalysis analogs to predict Antarctic and Southern Hemisphere climate changes. Quat. Sci. Rev. 155, 50–66.
Mayewski, P.A., Maasch, K.A., Yan, Y., Kang, S., Meyerson, E.A., Sneed, S.B., Kaspari, S.D., Dixon, D.A., Osterberg, E.C., Morgan, V.I., van Ommen, T., Curran, M.A.J., 2005. Solar forcing of the polar atmosphere. Ann. Glaciol. 41, 147–154.
Mayewski, P.A., Meeker, L.D., Twickler, M.S., Whitlow, S., Yang, Q., Prentice, M., 1997. Major features and forcing of high latitude Northern Hemisphere atmospheric circulation using a 110,000 year long glaciochemical series. J. Geophys. Res. 102, 26345–26366.
McGlone, M.S., Turney, C.S.M., Wilmshurst, J.M., Renwick, J., Pahnke, K., 2010. Divergent trends in land and ocean temperature in the Southern Ocean over the past 18,000 years. Nat. Geosci. 3, 622–626.
McKay, R., Naish, T., Carter, L., Riesselman, C., Dunbar, R., Sjunneskog, C., Winter, D., Sangiorgi, F., Warren, C., Pagani, M., Schouten, S., Willmott, V., Levy, R., DeConto, R., Powell, R.D., 2012. Antarctic and Southern Ocean influences on Late Pliocene global cooling. Proc. Natl. Acad. Sci. Unit. States Am. 109, 6423–6428. https://doi.org/10.1073/pnas.1112248109.
McKinnon, K.A., Mackintosh, A.N., Anderson, B.M., Barrell, D.J.A., 2012. The influence of sub-glacial bed evolution on ice extent: a model-based evaluation of the Last Glacial Maximum Pukaki glacier, New Zealand. Quat. Sci. Rev. 57, 46–57.
Mercer, J.H., 1976. Glacial history of southernmost South America. Quat. Res. 6 (2), 125–166.
Mercer, J.H., 1984. Simultaneous climatic change in both hemispheres and similar bipolar warming: Evidence and implications. In: Hansen, J.E., Takahashi, T. (Eds.), Climate Processes and Climate Sensitivity. American Geophysical Union, Washington. D. C., pp. 307–313
Mercer, J.H., Sutter, J.F., 1982. Late Miocene—earliest Pliocene glaciation in southern Argentina: Implications for global ice-sheet history. Palaeogeogr. Palaeoclimatol. Palaeoecol. 38, 185–206.
Milankovitch, M., 1941. Kanon der Erdbestrahlung und Seine Andwendung auf das Eiszeitenproblem (Belgrade).
Mix, A.C., Bard, E., Schneider, R., 2001. Environmental processes of the ice age: Land, oceans, glaciers (EPILOG). Quat. Sci. Rev. 20, 627–657.
Mohtadi, M., Hebbeln, D., 2004. Mechanisms and variations of the paleoproductivity off northern Chile (24°S-33°S) during the last 40,000 years. Paleoceanography 19, PA2023.
Monegato, G., Scardia, G., Hajdas, I., Rizzini, F., Piccin, A., 2017. The Alpine LGM in the boreal ice-sheets game. Sci. Rep. 7, 2078.
Monnin, E., Indermühle, A., Dällenbach, A., Flückiger, J., Stauffer, B., Stocker, T.F., Raynaud, D., Barnola, J.-M., 2001. Atmospheric CO_2 concentrations over the last glacial termination. Science 291, 112–114.
Moreno, P.I., Denton, G.H., Moreno, H., Lowell, T.V., Putnam, A.E., Kaplan, M.R., 2015. Radiocarbon chronology of the last glacial maximum and its termination in northwestern Patagonia. Quat. Sci. Rev. 122, 233–249.
Moreno, P.I., Lowell, T.V., Jacobson Jr., G.L., Denton, G.H., 1999. Abrupt vegetation and climate changes during the last glacial maximum and last termination in the Chilean Lake District: A case study from Canal de la Puntilla (41°S). Geogr. Ann. 81A, 285–311.
Mortimer, N., Campbell, H.J., Tulloch, A.J., King, P.R., Stagpoole, V.M., Wood, R.A., Rattenbury, M.S., Sutherland, R., Adams, C.J., Collot, J., Seton, M., 2017. Zealandia: Earth's hidden continent. GSA Today (Geol. Soc. Am.) 27, 27–35.
Munroe, J.S., Laabs, B.J.C., 2013. Temporal correspondence between pluvial lake highstands in the southwestern US and Heinrich Event 1. J. Quat. Sci. 28, 49–58.
Murphy, J.J., 1869. On the nature and cause of the glacial climate. Quaterly Journal of the Geological Society 25, 350–356.
National Institute of Water and Atmosphere – Taihoro Nukurangi, 2018. Special Climate Statement — Record Warmth in the Tasman Sea. New Zealand and Tasmania, p. 16.
Oliver, E.C.J., Benthuysen, J.A., Bindoff, N.L., Hobday, A.J., Holbrook, N.J., Mundy, C.N., Perkins-Kirkpatrick, S.E., 2017. The unprecedented 2015/16 Tasman Sea marine heatwave. Nat. Commun. 8, 16101.
Oliver, E.C.J., Lago, V., Hobday, A.J., Holbrook, N.J., Ling, S.D., Mundy, C.N., 2018. Marine heatwaves off eastern Tasmania: Trends, interannual variability, and predictability. Prog. Oceanogr. 161, 116–130.
Orsi, A.H., Whitworth, T., Nowlin, W.D., 1995. On the meridional extent and fronts of the Antarctic Circumpolar Current. Deep Sea Res. Oceanogr. Res. Pap. 42, 641–673. https://doi.org/10.1016/0967-0637(95)00021-W.
Pahnke, K., Zahn, R., Elderfield, H., Schulz, M., 2003. 340,000-year centennial-scale marine record of Southern Hemisphere climatic oscillation. Science 301, 948–952.
Palacios, D., Stokes, C.R., Phillips, F.M., Clague, J.J., Alcalá-Reygosa, J., Andrés, N., Angel, I., Blard, P.-H., Briner, J.P., Hall, B.L., Dahms, D., Hein, A.S., Jomelli, V.,

Mark, B.G., Martini, M.A., Moreno, P., Riedel, J., Sagredo, E., Stansell, N.D., Vázquez-Selem, L., Vuille, M., Ward, D.J., 2020. The deglaciation of the Americas during the last glacial termination. Earth Sci. Rev. 203, 103113.
Pedro, J.B., Bostock, H.C., Bitz, C.M., He, F., Vandergoes, M.J., Steig, E.J., Chase, B., Krause, C.E., Rasmussen, S.O., Markle, B.R., Cortese, G., 2016. The spatial extent and dynamics of the Antarctic Cold Reversal. Nat. Geosci. 9, 51–55.
Purdie, H., Anderson, B., Chinn, T., Owens, I., Mackintosh, A., Lawson, W., 2014. Franz Josef and Fox glaciers, New Zealand: Historic length records. Global Planet. Change 121, 41–52.
Putnam, A.E., 2015. A glacial zephyr. Nat. Geosci. 8, 175–176.
Putnam, A.E., Broecker, W.S., 2017. Human-induced changes in the distribution of rainfall. Science Advances 3, e160087.
Putnam, A.E., Denton, G.H., Schaefer, J.M., Barrell, D.J.A., Andersen, B.G., Finkel, R., Schwartz, R., Doughty, A.M., Kaplan, M., Schlüchter, C., 2010a. Glacier advance in southern middle latitudes during the Antarctic Cold Reversal. Nat. Geosci. 3, 700–704.
Putnam, A.E., Schaefer, J.M., Barrell, D.J.A., Vandergoes, M., Denton, G.H., Kaplan, M.R., Schwartz, R., Finkel, R.C., Goehring, B.M., Kelley, S.E., 2010b. In situ cosmogenic ^{10}Be production-rate calibration from the Southern Alps, New Zealand. Quat. Geochronol. 5, 392–409.
Putnam, A.E., Schaefer, J.M., Denton, G.H., Barrell, D.J.A., Andersen, B.G., Koffman, T.N.B., Rowan, A.V., Finkel, R.C., Rood, D.H., Schwartz, R., Vandergoes, M.J., Plummer, M.A., Brocklehurst, S.H., Kelley, S.E., Ladig, K.L., 2013a. Warming and glacier recession in the Rakaia valley, Southern Alps of New Zealand, during Heinrich Stadial 1. Earth Planet Sci. Lett. 382, 98–110.
Putnam, A.E., Schaefer, J.M., Denton, G.H., Barrell, D.J.A., Birkel, S.D., Andersen, B.G., Kaplan, M.R., Finkel, R.C., Schwartz, R., Doughty, A.M., 2013b. The Last Glacial Maximum at 44°S documented by a ^{10}Be moraine chronology at Lake Ohau, Southern Alps of New Zealand. Quat. Sci. Rev. 62, 114–141.
Putnam, A.E., Schaefer, J.M., Denton, G.H., Barrell, D.J.A., Finkel, R.C., Andersen, B.G., Schwartz, R., Chinn, T.J.H., Doughty, A.M., 2012. Regional climate control of glaciers in New Zealand and Europe during the pre-industrial Holocene. Nat. Geosci. 5, 627–630.
Rasmussen, S.O., Bigler, M., Blockley, S.P., Blunier, T., Buchardt, S.L., Clausen, H.B., Cvijanovic, I., Dahl-Jensen, D., Johnsen, S.J., Fischer, H., Gkinis, V., Guillevic, M., Hoek, W.Z., Lowe, J.J., Pedro, J.B., Popp, T., Seierstad, I.K., Steffensen, J.P., Svensson, A.M., Vellelonga, P., Vinther, B.M., Walker, M.J.C., Wheatley, J.J., Winstrup, M., 2014. A stratigraphic framework for abrupt climatic changes during the Last Glacial period based on three synchronized Greenland ice-core records: refining and extending the INTIMATE event stratigraphy. Quat. Sci. Rev. 106, 14–28.
Rasmussen, T.L., Thomsen, E., Moros, M., 2016. North Atlantic warming during Dansgaard-Oeschger events synchronous with Antarctic warming and out-of-phase with Greenland climate. Sci. Rep. 6, 20535.
Ravazzi, C., Badino, F., Marsetti, D., Patera, G., Reimer, P.J., 2012. Glacial to paraglacial history and forest recovery in the Oglio glacier system (Italian Alps) between 26 and 15 ka cal BP. Quat. Sci. Rev. 58, 146–161.
Ravazzi, C., Pini, R., Badino, F., De Amicis, M., Londeix, L., Reimer, P.J., 2014. The latest LGM culmination of the Garda Glacier (Italian Alps) and the onset of the glacial termination. Age of glacial collapse and vegetation chronosequence. Quat. Sci. Rev. 105, 26–47.
Reimer, P.J., Bard, E., Bayliss, A., Beck, J.W., Blackwell, P.G., Bronk Ramsay, C., Buck, C.E., Cheng, H., Edwards, R.L., Friedrich, M., Grootes, P., Guilderson, T.P., Haflidason, H., Hajdas, I., Hatté, C., Heaton, T.J., Hoffmann, D.L., Hogg, A.G., Hughen, K.A., Kaiser, K.F., Kromer, B., Manning, S.W., Niu, M., Reimer, R.W., Richards, D.A., Scott, E.M., Southon, J.R., Staff, R.A., Turney, C.S.M., van der Plicht, J., 2013. INTCAL13 and MARINE13 radiocarbon age calibration curves 0-50,000 years cal BP. Radiocarbon 55, 1869–1887.
Ridgway, K.R., 2007. Long-term trend and decadal variability of the southward penetration of the East Australian Current. Geophys. Res. Lett. 34, L13613.
Ridgway, K.R., Dunn, J.R., 2007. Observational evidence for a Southern Hemisphere oceanic supergyre. Geophys. Res. Lett. 34, L13612.
Röhl, K., 2006. Thermo-erosional notch development at fresh-water-calving Tasman Glacier, New Zealand. J. Glaciol. 52 (177), 203–213.
Rosell-Fieschi, M., Rintoul, S.R., Gourrion, J., Pelegrí, J.L., 2013. Tasman Leakage of intermediate waters as inferred from Argo floats. Geophys. Res. Lett. 40, 5456–5460.
Rowan, A.V., Plummer, M.A., Brocklehurst, S.H., Jones, M.A., Schultz, D.M., 2013. Drainage capture and discharge variations driven by glaciation in the Southern Alps, New Zealand. Geology 41, 199–202.
Russell, J.L., Dixon, K.W., Gnanadesikan, A., Stouffer, R.J., Toggweiler, J.R., 2006a. The Southern Hemisphere westerlies in a warming world: Propping open the door to the deep ocean. J. Clim. 19, 6382–6390.
Russell, J.L., Stouffer, R.J., Dixon, K.W., 2006b. Intercomparison of the Southern Ocean circulations in IPCC coupled model control simulations. J. Clim. 19, 4560–4575.
Saunders, K.M., Roberts, S.J., Perren, B., Butz, C., Sime, L., Davies, S., Van Nieuwenhuyze, W., Grosjean, M., Hodgson, D.A., 2018. Holocene dynamics of the Southern Hemisphere westerly winds and possible links to CO_2 outgassing. Nat. Geosci. 11, 650–655. https://doi.org/10.1038/s41561-018-0186-5.
Schaefer, J.M., Denton, G.H., Barrell, D.J.A., Ivy-Ochs, S., Kubik, P.W., Andersen, B.G., Phillips, F.M., Lowell, T.V., Schlüchter, C., 2006. Near-synchronous interhemispheric termination of the Last Glacial Maximum in mid-latitudes. Science 312, 1510–1513.
Schaefer, J.M., Denton, G.H., Kaplan, M., Putnam, A., Finkel, R.C., Barrell, D.J.A., Andersen, B.G., Schwartz, R., Mackintosh, A., Chinn, T., Schlüchter, C., 2009. High-frequency Holocene glacier fluctuations in New Zealand differ from the northern signature. Science 324, 622–625.
Schaefer, J.M., Putnam, A.E., Denton, G.H., Kaplan, M.R., Birkel, S.D., Doughty, A.M., Kelley, S.E., Barrell, D.J.A., Finkel, R.C., Winckler, G., Anderson, R.F., Ninnemann, U.S., Barker, S., Schwartz, R., Schleuchter, C., 2015. The southern glacial maximum 65,000 years ago and its unfinished termination. Quat. Sci. Rev. 114, 52–60.
Shulmeister, J., Goodwin, I., Renwick, J., Harle, K., Armand, L., McGlone, M.S., Cook, E., Dodson, J., Hesse, P.P., Mayewski, P., Curran, M., 2004. The Southern Hemisphere westerlies in the Australasian sector over the last glacial cycle: a synthesis. Quat. Int. 118–19, 23–53.
Shulmeister, J., Fink, D., Hyatt, O.M., Thackray, G.D., Rother, H., 2010. Cosmogenic ^{10}Be and ^{26}Al exposure ages of moraines in the Rakaia Valley, New Zealand and the nature of the last termination in New Zealand glacial systems. Earth Planet Sci. Lett. 297, 558–566.
Shulmeister, J., Thackray, G.D., Rittenour, T.M., Hyatt, O.M., 2018. Multiple glacial advances in the Rangitata Valley, South Island, New Zealand, imply roles for Southern Hemisphere westerlies and summer insolation in MIS 3 glacial advances. Quat. Res. 1–19.
Shulmeister, J., Thackray, G.D., Rittenour, T.M., Fink, D., Patton, N.R., 2019a. The timing and nature of the last glacial cycle in New Zealand. Quat. Sci. Rev. 206, 1–20.
Shulmeister, J., Fink, D., Winkler, S., Thackray, G.D., Borsellino, R., Hemmingsen, M., Rittenour, T.M., 2019b. Comment on Barrell et al. "Reconciling the onset of deglaciation in the Upper Rangitata valley, Southern Alps, New Zealand". Quat. Sci. Rev. 219, 312–315.
Siddall, M., Rohling, E.J., Almogi-Labin, A., Hemleben, C., Meischner, D., Schmelzer, I., Smeed, D.A., 2003. Sea-level fluctuations during the last glacial cycle. Nature 423, 853–858.
Sikes, E.L., Howard, W.R., Samson, C.R., Mahan, T.S., Robertson, L.G., Volkman, J.K., 2009. Southern Ocean seasonal temperature and Subtropical Front movement on the South Tasman Rise in the late Quaternary. Paleoceanography 24, PA2201.
Sime, L.C., Kohfeld, K.E., Le Quéré, C., Wolff, E.W., de Boerd, A.M., Graham, R.M., Boppe, L., 2013. Southern Hemisphere westerly wind changes during the Last Glacial Maximum: Model-data comparison. Quat. Sci. Rev. 64, 104–120.
Skinner, L.C., Fallon, S., Waelbroeck, C., Michel, E., Barker, S., 2010. Ventilation of the deep Southern Ocean and deglacial CO_2 rise. Science 328, 1147–1151.
Speich, S., Blanke, B., Cai, W., 2007. Atlantic Meridional Overturning Circulation and the Southern Hemisphere supergyre. Geophys. Res. Lett. 34.
Speich, S., Blanke, B., de Vries, P., Drijfhout, S., Döös, K., Ganachaud, A., Marsh, R., 2002. Tasman leakage: A new route in the global ocean conveyor belt. Geophys. Res. Lett. 29.
Speight, J.G., 1963. Late Pleistocene historical geomorphology of the Lake Pukaki area, New Zealand. N. Z. J. Geol. Geophys. 6, 160–188.
Stanford, J.D., Hemingway, R., Rohling, E.J., Challenor, P.G., Medina-Elizalde, M., Lester, A.J., 2011. Sea-level probability for the last deglaciation: A statistical analysis of far-field records. Global Planet. Change 79, 193–203.
Stone, J.O., 2000. Air pressure and cosmogenic isotope production. J. Geophys. Res. 105, 23753–23759.
Strand, P.D., Schaefer, J.M., Putnam, A.E., Denton, G.H., Barrell, D.J.A., Koffman, T.N.B., Schwartz, R., 2019. Millennial-scale pulsebeat of glaciation in the Southern Alps of New Zealand. Quat. Sci. Rev. 220, 165–177.
Strelin, J.A., Denton, G.H., Vandergoes, M.J., Ninnemann, U.S., Putnam, A.E., 2011. Radiocarbon chronology of the late-glacial Puerto Bandera moraines, Southern Patagonian Icefield, Argentina. Quat. Sci. Rev. 30, 2551–2569.
Stuiver, M., Grootes, P.M., 2000. GISP2 oxygen isotope ratios. Quat. Res. 53, 277–283.
Stuiver, M., Polach, H.A., 1977. Discussion of reporting ^{14}C data. Radiocarbon 19, 355–363.
Sutherland, J.L., Carrivick, J.L., Shulmeister, J., Quincey, D.J., James, W.H.M., 2019. Ice-contact proglacial lakes associated with the Last Glacial Maximum across the Southern Alps, New Zealand. Quat. Sci. Rev. 213, 67–92.
Sutherland, J.L., Carrivick, J.L., Gandy, N., Shulmeister, J., Quincey, D.J., Cornford, S.L., 2020. Proglacial lakes control glacier geometry and behavior during recession. Geophys. Res. Lett. 47, e2020GL088865 https://doi.org/10.1029/2020GL088865.
Toggweiler, J.R., 2009. Shifting westerlies. Science 323, 1434–1435.
Toggweiler, J.R., Russell, J., 2008. Ocean circulation in a warming climate. Nature 451, 286–288.
Toggweiler, J.R., Russell, J.L., Carson, S.R., 2006. Midlatitude westerlies, atmospheric CO_2, and climate change during the ice ages. Paleoceanography 21, PA2005.
Toucanne, S., Soulet, G., Freslon, N., Silva Jacinto, R., Dennielou, B., Zaragosi, S., Eynaud, F., Bourillet, J.-F., Bayon, G., 2015. Millennial-scale fluctuations of the European Ice Sheet at the end of the last glacial, and their potential impact on global climate. Quat. Sci. Rev. 123, 113–133.
Turney, C.S.M., Jones, R.T., 2010. Does the Agulhas Current amplify global temperatures during super-interglacials? J. Quat. Sci. 25, 839–843.
van Husen, D., 1997. LGM and late-glacial fluctuations in the Eastern Alps. Quat. Int. 38–39, 109–118.
van Sebille, E., Sprintall, J., Schwarzkopf, F.U., Sen Gupta, A., Santoso, A., England, M.H., Biastoch, A., Böning, C.W., 2014. Pacific-to-Indian Ocean connectivity: Tasman leakage, Indonesian Throughflow, and the role of ENSO. J. Geophys. Res.: Oceans 119, 1365–1382.
Vandergoes, M.J., Newnham, R.M., Denton, G.H., Blaauw, M., Barrell, D.J.A., 2013. The anatomy of Last Glacial Maximum climate variations in south Westland, New

Zealand, derived from pollen records. Quat. Sci. Rev. 74, 215–229.
Wang, X., Auler, A.S., Edwards, R.L., Cheng, H., Ito, E., Wang, Y., Kong, X., Solheid, M., 2007. Millennial-scale precipitation changes in southern Brazil over the past 90,000 years. Geophys. Res. Lett. 34, L23701.
Wang, X.F., Auler, A.S., Edwards, R.L., Cheng, H., Cristalli, P.S., Smart, P.L., Richards, D.A., Shen, C.C., 2004. Wet periods in northeastern Brazil over the past 210 kyr linked to distant climate anomalies. Nature 432, 740–743.
Wang, Y., Cheng, H., Edwards, R.L., Kong, X., Shao, X., Chen, S., Wu, J., Jiang, X., Wang, X., An, Z., 2008. Millennial- and orbital-scale changes in the East Asian monsoon over the past 224,000 years. Nature 451, 1090–1093.
Wang, Y.J., Cheng, H., Edwards, R.L., An, Z.S., Wu, J.Y., Shen, C.C., Dorale, J.A., 2001. A high-resolution absolute-dated Late Pleistocene monsoon record from Hulu Cave, China. Science 294, 2345–2348.
Wirsig, C., Zasadni, J., Christl, M., Akçar, N., Ivy-Ochs, S., 2016a. Dating the onset of LGM ice surface lowering in the High Alps. Quat. Sci. Rev. 143, 37–50.
Wirsig, C., Zasadni, J., Ivy-Ochs, S., Christl, M., Kober, F., Schlüchter, C., 2016b. A deglaciation model of the Oberhasli, Switzerland. J. Quat. Sci. 31, 46–59.